Progress In Electromagnetics Research, Vol. 135, 527–562, 2013

EFFECT OF THRESHOLD VALUE ON THE PERFORMANCE OF NATURAL FREQUENCY-BASED RADAR TARGET RECOGNITION

Sung-Woo Cho and Joon-Ho Lee*

Department of Information and Communication Engineering, Sejong University, Seoul, Korea

Abstract—In this paper, the performance analysis of the natural frequency-based radar target recognition in the time domain is considered. We investigate the dependence of the probability of correct classification on a specific threshold value, and determine the optimum threshold value for two targets, and the sub-optimal threshold for multiple targets to maximize the probability of correct classification. Based on the probability density function (PDF) of some quantity consisting of the projections of the late time response onto the column spaces of the matrices constructed using the natural frequencies of the specific targets, we propose how to determine an optimum threshold in the sense that the probability of correct classification of two targets is maximized. By extending the scheme for two targets, we show how to determine a threshold value close to the optimal threshold for multiple targets. The scheme is validated by comparing the performance using the analytic method with that using the Monte-Carlo simulation.

1. INTRODUCTION

Radar [1–25] has been widely used as a sensor for detection [26–46] and tracking [17, 47–49] of radar target. The range to the target and the velocity of the target can be measured using radar. Doppler shift can be used to estimate the velocity of moving target [26–28, 50, 51]. The radar cross section (RCS) [52–59] of radar target can be estimated from the strength of the signal reflected from the target. The reflected signal of the radar target can be simulated using scattering analysis of the radar target [60–69]. In addition to radar detection and tracking, there have been many studies on radar target recognition [70–80, 159–166].

Received 31 October 2012, Accepted 27 December 2012, Scheduled 2 January 2013
* Corresponding author: Joon-Ho Lee (joonhlee@sejong.ac.kr).

There are many radar signatures which can be used for radar target recognition: Natural frequencies of radar target [159–166], high resolution range (HRR) profiles [72, 75–80] of radar target, microwave image [101–123] of the radar target [1, 26, 31, 50, 55, 70, 73, 81–100], and inverse synthetic aperture radar (ISAR) [55, 86–100, 125, 126] image proved to be useful features for target recognition. Jet engine modulation and helicopter modulation [127, 128] have also been known as useful features for target recognition.

It has been shown that the performance of radar target recognition can be improved by exploiting the polarization characteristics [1, 31, 71, 84, 129]. In the viewpoint of the anti-stealth technology, detection of low RCS target has been an interest. Multiple-input and multiple-output (MIMO) radar, bistatic radar and multi-static radar [51, 84, 85, 124, 130–137] have been employed to detect low-RCS target. Pulse compression proved to be an effective way to enhance the performance of radar target detection and recognition [138–140]. In addition, ultra-wideband (UWB) radar [71, 89, 141–146] has been employed to improve the performance.

There have been many studies in the literature about radar target detection [148–155, 169] and recognition [70, 159–166]. The first set of works presents how different techniques have been successfully applied to detect radar targets in different environments such as sea [152, 153] and ground [154, 155]. The typical techniques are neural-network based detectors [148, 149] and constant false alarm rate (CFAR) detectors [150, 151]. The works of the second set [148–164] present how the above-mentioned or other techniques have been successfully applied in radar target recognition tasks. Natural frequency is a commonly used radar signature for radar target recognition [159–162, 163–167].

In [160, 161], the authors presented the natural frequency-based radar target recognition scheme in the time domain [160] and in the frequency domain [161]. In [162] and [168], performance of natural frequency-based target recognition has been analyzed in the time domain and in the frequency domain, respectively. The schemes are based on the binary hypothesis testing and a numerical evaluation of a probability density function (PDF).

In this paper, based on the results in [162], we consider how to improve the probability of correct classification by properly selecting the threshold value used for the classification.

2. LATE TIME RESPONSE AND NATURAL FREQUENCIES

Let $y_{n|k}$ represent a sampled response with sampling interval of Δt, and define $z_{m|k} = \exp[s_{m|k}\Delta t]$, where $s_{1|k}, \ldots, s_{M_k|k}$ are the natural frequencies of the k-th target. M_k is the number of the natural frequencies of target k. It can be easily shown that, based on the late time representation using the natural frequencies, the late time response can be written as [160], for the k-th target,

$$y_{n|k} = u_{n|k} + g_{n|k} = \sum_{m=1}^{M_k} c_{m|k} {z_{m|k}}^n + g_{n|k} \quad n = 1, 2, \ldots, N \tag{1}$$

where N is the number of the sampled frequency response.

$g_{n|k}$ is the zero-mean Gaussian distributed with variance of σ^2, associated with $y_{n|k}$. $s_{m|k}$, $m = 1, \ldots, M_k$, is the natural frequency of the k-th target. $u_{n|k}$, $n = 1, \ldots, N$, is the noiseless late time response of the k-th target.

If we define

$$\mathbf{y}_k = \begin{bmatrix} y_{1|k} & y_{2|k} & \cdots & y_{N|k} \end{bmatrix}^{\mathrm{T}} \tag{2}$$

$$\mathbf{c}_k = \begin{bmatrix} c_{1|k} & c_{2|k} & \cdots & c_{M_k|k} \end{bmatrix}^{\mathrm{T}} \tag{3}$$

$$\mathbf{g}_k = \begin{bmatrix} g_{1|k} & g_{2|k} & \cdots & g_{N|k} \end{bmatrix}^{\mathrm{T}} \tag{4}$$

$$\mathbf{u}_k = \begin{bmatrix} u_{1|k} & u_{2|k} & \cdots & u_{N|k} \end{bmatrix}^{\mathrm{T}}, \tag{5}$$

Equation (1) can be written as

$$\mathbf{y}_k = \mathbf{B}_k\mathbf{c}_k + \mathbf{g}_k = \mathbf{u}_k + \mathbf{g}_k \tag{6}$$

where $\{\mathbf{B}_k\}_{nm}$ is defined as

$$\{\mathbf{B}_k\}_{nm} = {z_{m|k}}^n. \tag{7}$$

3. MOTIVATION

In [162], the authors chose zero for the threshold for the classification. Assume that we try to recognize target 1 and target 2 based on the PDF of

$$Z_{21|k} \equiv \|\mathbf{P}_2\mathbf{y}_k\|^2 - \|\mathbf{P}_1\mathbf{y}_k\|^2 = \mathbf{y}_k^{\mathrm{H}}\mathbf{P}_2\mathbf{y}_k - \mathbf{y}_k^{\mathrm{H}}\mathbf{P}_1\mathbf{y}_k \underset{\text{target 1}}{\overset{\text{target 2}}{\gtrless}} 0 \quad k = 1, 2 \tag{8}$$

where k denotes that the noisy late time response is from the k-th target and the projection matrices $\mathbf{P}_1$ and $\mathbf{P}_2$ are defined as

$$\mathbf{P}_2 = \mathbf{B}_2\left(\mathbf{B}_2^{\mathrm{H}}\mathbf{B}_2\right)^{-1}\mathbf{B}_2^{\mathrm{H}} \tag{9}$$

$$\mathbf{P}_1 = \mathbf{B}_1\left(\mathbf{B}_1^{\mathrm{H}}\mathbf{B}_1\right)^{-1}\mathbf{B}_1^{\mathrm{H}}. \tag{10}$$

Eigendecomposition of $\mathbf{P}_2 - \mathbf{P}_1$ results in

$$\mathbf{P}_2 - \mathbf{P}_1 = \mathbf{V}\mathbf{\Lambda}_{21}\mathbf{V}^{\mathrm{H}}. \tag{11}$$

$\mathbf{w}_k$ is defined from

$$\mathbf{w}_k = \begin{bmatrix} w_{1|k} & \dots & w_{N|k} \end{bmatrix} = \mathbf{V}^{\mathrm{H}}\mathbf{y}_k. \tag{12}$$

The mean of $\mathbf{w}_k$ is denoted as

$$\mathrm{mean}(\mathbf{w}_k) = \begin{bmatrix} \mu_{1|k} & \dots & \mu_{N|k} \end{bmatrix} = \mathbf{V}^{\mathrm{H}}\mathbf{u}_k. \tag{13}$$

$Z_{21|k}$ in Eq. (8) can be written as [162, 170]

$$Z_{21|k} = F_{21|k} + G_{21|k} \tag{14}$$

where

$$F_{21|k} = \sum_{l=1}^{M_2-M_1} {w_{l|k}}^2 \quad \text{and} \quad G_{21|k} = \sum_{l=1}^{2M_1} \lambda_l {w_{M_2-M_1+l|k}}^2. \tag{15}$$

The characteristic functions of $F_{21|k}$ and $G_{21|k}$ are [162]

$$\Phi_{F_{21|k}}(j\omega) = \frac{1}{(1-j2\omega\sigma^2)^{(M_2-M_1)/2}} \exp\left(\frac{j\omega \sum\limits_{l=1}^{M_2-M_1} \mu_{l|k}^2}{1-j2\omega\sigma^2} \right) \tag{16}$$

$$\Phi_{G_{21|k}}(j\omega) = \prod_{l=1}^{2M_1} \frac{\lambda_l}{|\lambda_l| \, (1-j2\omega\lambda_l\sigma^2)^{\frac{1}{2}}} \exp\left(\frac{j\omega\mu_{M_2-M_1+l|k}^2 \lambda_l}{1-j2\omega\lambda_l\sigma^2} \right). \tag{17}$$

Finally, the PDF of $Z_{21|k}$ is

$$p_{Z_{21|k}}(z) = F^{-1}\left\{ \Phi_{F_{21|k}}(j\omega)\Phi_{G_{21|k}}(j\omega) \right\}. \tag{18}$$

The cumulative distribution function (CDF) of $Z_{21|k}$ is obtained from

$$F_{Z_{21|k}}(z) = \int_{-\infty}^{z} p_{Z_{21|k}}\left(z'\right) dz'. \tag{19}$$

The performance analysis of the natural frequency-based radar target recognition in the frequency domain is considered in this paper. In the scheme presented in [162], the authors set the threshold for the classification to zero. In this paper, we propose to change the threshold value to see what threshold value results in the maximum probability of correct classification.

In addition, we show how to determine the optimum threshold from the analytic PDF's and CDF's for two targets. For more than two targets, we propose how to choose a threshold value which is very close to the optimum threshold $\gamma_{\mathrm{opt}}^{\mathrm{simul}}$ maximizing Eq. (25).

$\mathbf{P}_2\mathbf{y}$ should be a vector on the column space of $\mathbf{B}_2$ since $\mathbf{P}_2\mathbf{y}$ is a projection of $\mathbf{y}$ onto the column space of $\mathbf{B}_2$. Similarly, $\mathbf{P}_1\mathbf{y}$ should be on the column space of $\mathbf{B}_1$.

For $M_1 < M_2$, the dimension of the column space of $\mathbf{B}_2$ is greater than that of the column space of $\mathbf{B}_1$.

Note that the ranks of $\mathbf{B}_1$ and $\mathbf{B}_2$ are M_1 and M_2, respectively. For $M_1 < M_2$, the constraint that the projection should be on the column space of $\mathbf{B}_2$ is less demanding than the constraint that the projection should be on the column space of $\mathbf{B}_1$.

For $M_1 < M_2$, $\|\mathbf{P}_2\mathbf{y}\|$ tends to be larger and $\|\mathbf{P}_1\mathbf{y}\|$ tends to be smaller both for $\mathbf{y} = \mathbf{y}_1$ and $\mathbf{y} = \mathbf{y}_2$.

$\|\mathbf{P}_2\mathbf{y}\|$ gets smaller for smaller M_2, and vice versa, and $\|\mathbf{P}_1\mathbf{y}\|$ gets smaller for smaller M_1, and vice versa.

The constraint that the projection should be on the column space of $\mathbf{B}_2$ gets stricter resulting in smaller $\|\mathbf{P}_2\mathbf{y}\|$ as M_2 gets smaller, and vice versa. Similarly, the constraint associated with $\mathbf{P}_1\mathbf{y}$ gets stricter resulting in smaller $\|\mathbf{P}_1\mathbf{y}\|$ as M_1 gets smaller, and vice versa.

$\mathrm{Prob}(\|\mathbf{P}_2\mathbf{y}\| > \|\mathbf{P}_1\mathbf{y}\|)$ for $M_2 > M_1$ becomes larger than $\mathrm{Prob}(\|\mathbf{P}_2\mathbf{y}\| > \|\mathbf{P}_1\mathbf{y}\|)$ for $M_2 = M_1$, and $\mathrm{Prob}(\|\mathbf{P}_2\mathbf{y}\| < \|\mathbf{P}_1\mathbf{y}\|)$ for $M_2 > M_1$ becomes smaller than $\mathrm{Prob}(\|\mathbf{P}_2\mathbf{y}\| < \|\mathbf{P}_1\mathbf{y}\|)$ for $M_2 = M_1$.

What we suggest in this paper is to improve $P_I(\gamma)$ by defining

$$P_{I|1}(\gamma) = \mathrm{Prob}\left(\left(\|\mathbf{P}_2\mathbf{y}\|^2 - \|\mathbf{P}_1\mathbf{y}\|^2\right) < \gamma|\text{1st target is present}\right) \quad (20)$$

$$P_{I|2}(\gamma) = \mathrm{Prob}\left(\left(\|\mathbf{P}_2\mathbf{y}\|^2 - \|\mathbf{P}_1\mathbf{y}\|^2\right) > \gamma|\text{2nd target is present}\right) \quad (21)$$

$$\begin{aligned} P_I(\gamma) &= \sum_{k=1}^{2} P_{I|k}(\gamma)\mathrm{Prob}(k\text{-th target is present}) \\ &= \frac{1}{2}\sum_{k=1}^{2}\left(P_{I|1}(\gamma) + P_{I|2}(\gamma)\right). \end{aligned} \quad (22)$$

The simulation performance can be written as

$$P_{I|1}^{\mathrm{simul}}(\gamma) = \mathrm{Prob}\left(\left(\|\mathbf{P}_2\mathbf{y}_1\|^2 - \|\mathbf{P}_1\mathbf{y}_1\|^2\right) < \gamma\right) \quad (23)$$

$$P_{I|2}^{\mathrm{simul}}(\gamma) = \mathrm{Prob}\left(\left(\|\mathbf{P}_2\mathbf{y}_2\|^2 - \|\mathbf{P}_1\mathbf{y}_2\|^2\right) > \gamma\right) \quad (24)$$

$$P_I^{\mathrm{simul}}(\gamma) = \sum_{k=1}^{2} P_{I|k}^{\mathrm{simul}}(\gamma)\mathrm{Prob}(k\text{-th target is present})$$

$$
\begin{aligned}
&= \frac{1}{2}\sum_{k=1}^{2} P_{I\,|k}^{\text{simul}}(\gamma) \\
&= \frac{1}{2}\left[\text{Prob}\left(\left(\|\mathbf{P}_2\mathbf{y}_1\|^2 - \|\mathbf{P}_1\mathbf{y}_1\|^2\right) < \gamma\right)\right. \\
&\quad \left. +\text{Prob}\left(\left(\|\mathbf{P}_2\mathbf{y}_2\|^2 - \|\mathbf{P}_1\mathbf{y}_2\|^2\right) > \gamma\right)\right] \qquad (25)
\end{aligned}
$$

where $\|\mathbf{P}_2\mathbf{y}_1\|^2$, $\|\mathbf{P}_1\mathbf{y}_1\|^2$, $\|\mathbf{P}_2\mathbf{y}_2\|^2$ and $\|\mathbf{P}_1\mathbf{y}_2\|^2$ are obtained from the Monte-Carlo simulation in the sense that the noises in $\mathbf{y}_1$ and $\mathbf{y}_2$ are Gaussian random vectors.

By setting $\gamma = 0$ in Eq. (23) and Eq. (24), we get $P_{I|1}$ and $P_{I|2}$ defined in the scheme presented in [162].

4. DEPENDENCE OF $\mathbf{P_I}$ ON γ FOR TWO TARGETS

Let $P_{I|2}(\gamma)$ be the probability of correct classification with the specified threshold value of γ given that the second target is present and $P_{I|1}(\gamma)$ be the probability of correct classification with the specified threshold value of γ given that the first target is present.

The probability of correct classification with threshold value γ is obtained from the PDF as follows:

$$
\begin{aligned}
P_{I|1}^{\text{analy}}(\gamma) &= \text{Prob}(Z_{21|k} < \gamma\,|k = 1) \\
&= \int_{-\infty}^{\gamma} p_{Z_{21|1}}(z)dz = F_{Z_{21|1}}(\gamma) \qquad (26) \\
P_{I|2}^{\text{analy}}(\gamma) &= \text{Prob}(Z_{21|k} > \gamma\,|k = 2) \\
&= \int_{\gamma}^{\infty} p_{Z_{21|2}}(z)dz = 1 - F_{Z_{21|2}}(\gamma) \qquad (27)
\end{aligned}
$$

$$
\begin{aligned}
P_I^{\text{analy}}(\gamma) &= \sum_{k=1}^{2} P_{I\,|k}^{\text{analy}}(\gamma)\text{Prob}(k\text{-th target is present}) \\
&= \frac{1}{2}\sum_{k=1}^{2} P_{I\,|\,k}(\gamma) = \frac{1}{2}(F_{Z_{21|1}}(\gamma) + 1 - F_{Z_{21|2}}(\gamma)) \qquad (28)
\end{aligned}
$$

where $F_{Z_{21|1}}(z)$ and $F_{Z_{21|2}}(z)$ represent the CDF of $Z_{21|k=1}$ and $Z_{21|k=2}$, respectively. Refer to Section 3 to see how to numerically evaluate the PDF's and the CDF's of $Z_{21|1}$ and $Z_{21|2}$ [162].

As we change γ in Eq. (28) with respect to γ, the optimum threshold value, γ_{opt} can be determined from the threshold value at which $P_I(\gamma)$ is maximized.

From Eq. (26) and Eq. (27), $P_{I|1}^{\text{analy}}(\gamma)$ and $P_{I|2}^{\text{analy}}(\gamma)$ are monotonic increasing and decreasing functions of γ, respectively. Since $P_{I}^{\text{analy}}(\gamma)$ is a sum of monotonic increasing and decreasing functions, it is quite intuitive to see that $P_I(\gamma)$ tends to have a local maximum at $\gamma = \gamma_{\text{opt}}$.

γ_{opt} can also be analytically found by differentiating $P_I(\gamma)$ with respect to γ:

$$\begin{aligned}
\frac{d}{d\gamma} P_{\text{I}}^{\text{analy}}(\gamma) &= 0 \\
\frac{d}{d\gamma}\left(\frac{1}{2}\left(P_{\text{I}|1}^{\text{analy}}(\gamma)+P_{\text{I}|2}^{\text{analy}}(\gamma)\right)\right) &= \frac{1}{2}\frac{d}{d\gamma}\left(1-F_{Z_{21|2}(\gamma)}+F_{Z_{21|1}(\gamma)}\right) \\
&= \frac{1}{2}\left(-p_{Z_{21|2}(\gamma)}+p_{Z_{21|1}(\gamma)}\right) = 0 \\
p_{Z_{21|2}(\gamma)} &= p_{Z_{21|1}(\gamma)}.
\end{aligned} \tag{29}$$

Therefore, γ_{opt} can be found from γ value satisfying Eq. (29).

Let ζ_1 and ζ_2 denote the limit above which the values of $p_{Z_{21|1}}$ and $p_{Z_{21|2}}$ can be practically set to be zero, respectively, which can be given, for $k = 1, 2$, [162]

$$\begin{aligned}
\zeta_k &= \mu_{Z_{21|k}} + 6\sigma_{Z_{21|k}}, && \mu_{Z_{21|k}} > 0 \\
\zeta_k &= -\left(\mu_{Z_{21|k}} - 6\sigma_{Z_{21|k}}\right), && \mu_{Z_{21|k}} < 0.
\end{aligned} \tag{30}$$

Using Eq. (30), the range of γ over which $P_I(\gamma)$ should be calculated is given by

$$-\max(\zeta_1, \zeta_2) < \gamma < \max(\zeta_1, \zeta_2). \tag{31}$$

5. DEPENDENCE OF P_I ON γ FOR THREE TARGETS

For simplicity, we assume that there are three targets. We can extend the results to more than three targets.

For three targets, we tabulate the decision strategy for nonzero threshold γ in Table 1: Notation I is the convention used for two targets and Notation II and Notation III are the conventions used for more than two targets.

Note that in Table 1, for derivation of Notation II from Notation I, we use the fact that, for example, $Z_{31|1} < \gamma$ is equivalent to $Z_{13|1} > -\gamma$ due to $Z_{31|1} = -Z_{13|1}$. In general, $Z_{ik|k} < \gamma$ is equivalent to $Z_{ki|k} > -\gamma$ because of $Z_{ik|k} = -Z_{ki|k}$.

If we define

$$t_{kl|k}(\gamma) = \begin{cases} \gamma, & k > l \\ -\gamma, & k < l, \end{cases} \tag{32}$$

Table 1. Decision strategy for three targets.

targets	Notation I	Notation II	Notation III
1 2	$Z_{21\|2} > \gamma$, $Z_{21\|1} < \gamma$,	$Z_{21\|2} > \gamma$ $Z_{12\|1} > -\gamma$	$Z_{21\|2} > t_{21\|2}(\gamma)$ $Z_{12\|1} > t_{12\|1}(\gamma)$
1 2	$Z_{31\|3} > \gamma$, $Z_{31\|1} < \gamma$,	$Z_{31\|3} > \gamma$ $Z_{13\|1} > -\gamma$	$Z_{31\|3} > t_{31\|3}(\gamma)$ $Z_{13\|1} > t_{13\|1}(\gamma)$
1 2	$Z_{32\|3} > \gamma$, $Z_{32\|2} < \gamma$,	$Z_{32\|3} > \gamma$ $Z_{23\|2} > -\gamma$	$Z_{32\|3} > t_{32\|3}(\gamma)$ $Z_{23\|2} > t_{23\|2}(\gamma)$

we get Notation III from Notation II in Table 1.

From Table 1, the probability of correct identification can be written as

$$P_{I|1}(\gamma) = \text{Prob}\left\{Z_{12|1} > t_{12|1}(\gamma), Z_{13|1} > t_{13|1}(\gamma)\right\} \tag{33}$$

$$P_{I|2}(\gamma) = \text{Prob}\left\{Z_{21|2} > t_{21|2}(\gamma), Z_{23|2} > t_{23|2}(\gamma)\right\} \tag{34}$$

$$P_{I|3}(\gamma) = \text{Prob}\left\{Z_{31|3} > t_{31|3}(\gamma), Z_{32|3} > t_{32|3}(\gamma)\right\}. \tag{35}$$

Using Eq. (32) in Eq. (33)–Eq. (35), we have

$$P_{I|1}(\gamma) = \text{Prob}\left\{Z_{12|1} > -\gamma, Z_{13|1} > -\gamma\right\} \tag{36}$$

$$P_{I|2}(\gamma) = \text{Prob}\left\{Z_{21|2} > \gamma, Z_{23|2} > -\gamma\right\} \tag{37}$$

$$P_{I|3}(\gamma) = \text{Prob}\left\{Z_{31|3} > \gamma, Z_{32|3} > \gamma\right\}. \tag{38}$$

6. DEPENDENCE OF $\mathbf{P_I}$ ON γ FOR MULTIPLE TARGETS

Equations (33)–(35) are valid for three targets. It is straightforward to extend Eq. (33)–Eq. (35) to more than three targets. Assume that there are Q targets.

Assuming that the k-th target is present, the probability of correct classification can be written as, for $k = 1, \ldots, Q$,

$$\begin{aligned} P_{I|k}(\gamma) = \text{Prob}\big(&Z_{k1|k} > t_{k1|k}(\gamma), \ldots, Z_{k,k-1|k} > t_{k,k-1|k}(\gamma)\,, \\ &Z_{k,k+1|k} > t_{k,k+1|k}(\gamma), \ldots, Z_{k,Q|k} > t_{k,Q|k}(\gamma)\big). \end{aligned} \tag{39}$$

Using Eq. (32) in Eq. (39), we have

$$\begin{aligned} P_{I|k}(\gamma) = \text{Prob}\big(&Z_{k1|k} > \gamma, \ldots, Z_{k,k-1|k} > \gamma \\ &Z_{k,k+1|k} > -\gamma, \ldots, Z_{k,Q|k} > -\gamma\big). \end{aligned} \tag{40}$$

$Z_{kl|k}$ and $Z_{lk|k}$ are defined as

$$Z_{kl|k} \equiv \|\mathbf{P}_k \mathbf{y}_k\|^2 - \|\mathbf{P}_l \mathbf{y}_k\|^2 \tag{41}$$

$$Z_{lk|k} \equiv \|\mathbf{P}_l \mathbf{y}_k\|^2 - \|\mathbf{P}_k \mathbf{y}_k\|^2 . \tag{42}$$

Note that Eq. (41) and Eq. (42) are consistent with Eq. (8).

Using Eq. (41) and Eq. (42) in Eq. (40), the probability of classification can be expressed as

$$\begin{aligned} P_{I\,|\,k}(\gamma) = \text{Prob}\,\big[&\mathbf{y}^{\mathrm{H}}\mathbf{P}_k\mathbf{y} > \mathbf{y}^{\mathrm{H}}\mathbf{P}_1\mathbf{y} + \gamma, \ldots, \mathbf{y}^{\mathrm{H}}\mathbf{P}_k\mathbf{y} \\ &> \mathbf{y}^{\mathrm{H}}\mathbf{P}_{k-1}\mathbf{y} + \gamma, \mathbf{y}^{\mathrm{H}}\mathbf{P}_k\mathbf{y} > \mathbf{y}^{\mathrm{H}}\mathbf{P}_{k+1}\mathbf{y} - \gamma, \ldots, \mathbf{y}^{\mathrm{H}}\mathbf{P}_k\mathbf{y} \\ &> \mathbf{y}^{\mathrm{H}}\mathbf{P}_Q\mathbf{y} - \gamma \,|k\text{th target}\big] . \end{aligned} \tag{43}$$

Since evaluating Eq. (43) is quite challenging, we try to get the upper bound and the lower bound of the probability of correct classification.

Assuming that the correct target is the k-th target, the upper bound and the lower bound of correct classification are given by [137]

$$P^{\mathrm{up}}_{I\,|\,k}(\gamma) = \min_{i \neq k} \left\{ \int_{t_{ki|k}(\gamma)}^{\infty} p_{Z_{ki|k}}(z) dz \right\} = \min_{i \neq k} \left\{ 1 - F_{Z_{ki|k}}(t_{ki|k}(\gamma)) \right\} \tag{44}$$

$$\begin{aligned} P^{\mathrm{lo}}_{I\,|\,k}(\gamma) &= \max \left\{ 0, 1 - \sum_{\substack{i=1 \\ i \neq k}}^{Q} \int_{-\infty}^{t_{ki|k}(\gamma)} p_{Z_{ki|k}}(z) dz \right\} \\ &= \max \left\{ 0, 1 - \sum_{\substack{i=1 \\ i \neq k}}^{Q} F_{Z_{ki|k}}(t_{ki|k}(\gamma)) \right\} . \end{aligned} \tag{45}$$

where $F_{Z_{ki|k}}(z)$ denotes the CDF of $Z_{ki|k}$.

Note that, the PDF's and the CDF's in Eq. (44)–Eq. (45) are evaluated using the scheme in Section 4.

Simulation performance based on the Monte-Carlo simulation is

$$\begin{aligned} P^{\mathrm{simul}}_{I|k}(\gamma) = \text{Prob}\,\big[\,&\mathbf{y}_{\mathbf{k}}^{\mathrm{H}}\mathbf{P}_k\mathbf{y}_{\mathbf{k}} > \mathbf{y}_{\mathbf{k}}^{\mathrm{H}}\mathbf{P}_1\mathbf{y}_{\mathbf{k}} + t_{k1|k}(\gamma), \ldots, \mathbf{y}_{\mathbf{k}}^{\mathrm{H}}\mathbf{P}_k\mathbf{y}_{\mathbf{k}} \\ &> \mathbf{y}_{\mathbf{k}}^{\mathrm{H}}\mathbf{P}_{k-1}\mathbf{y}_{\mathbf{k}} + t_{k,k-1|k}(\gamma), \mathbf{y}_{\mathbf{k}}^{\mathrm{H}}\mathbf{P}_k\mathbf{y}_{\mathbf{k}} > \mathbf{y}_{\mathbf{k}}^{\mathrm{H}}\mathbf{P}_{k+1}\mathbf{y}_{\mathbf{k}} \\ &+ t_{k,\,k+1|k}(\gamma), \ldots, \mathbf{y}_{\mathbf{k}}^{\mathrm{H}}\mathbf{P}_k\mathbf{y}_{\mathbf{k}} > \mathbf{y}_{\mathbf{k}}^{\mathrm{H}}\mathbf{P}_Q\mathbf{y}_{\mathbf{k}} + t_{k,Q|k}(\gamma)\big] . \end{aligned} \tag{46}$$

The upper bound and the lower bound of correct classification, considering all Q targets, are given by [162]

$$P_I^{\mathrm{up}}(\gamma) = \frac{1}{Q}\sum_{k=1}^{Q} P_{I\,|\,k}^{\mathrm{up}}(\gamma) \tag{47}$$

$$P_{\mathrm{I}}^{\mathrm{lo}}(\gamma) = \frac{1}{Q}\sum_{k=1}^{Q} P_{I\,|\,k}^{\mathrm{lo}}(\gamma). \tag{48}$$

Simulation performance considering all Q targets is

$$P_I^{\mathrm{simul}}(\gamma) = \frac{1}{Q}\sum_{k=1}^{Q} P_{I|k}^{\mathrm{simul}}(\gamma). \tag{49}$$

Using Eq. (45) in Eq. (48), we can plot $P_I^{\mathrm{up}}(\gamma)$ as we change γ. From the plot, we can easily identify the optimum threshold, $\gamma_{\mathrm{opt}}^{\mathrm{lo}}$, at which $P_{\mathrm{I}}^{\mathrm{lo}}(\gamma)$ is maximized:

$$\gamma_{\mathrm{opt}}^{\mathrm{lo}} \equiv \arg\max_{\gamma} P_I^{\mathrm{lo}}(\gamma). \tag{50}$$

Similarly, using Eq. (44) in Eq. (47), we can calculate $P_I^{\mathrm{up}}(\gamma)$ for various γ values and the optimum threshold value, $\gamma_{\mathrm{opt}}^{\mathrm{up}}$, can be found from the threshold value at which $P_{\mathrm{I}}^{\mathrm{up}}(\gamma)$ achieves the maximum.

$$\gamma_{\mathrm{opt}}^{\mathrm{up}} \equiv \arg\max_{\gamma} P_I^{\mathrm{up}}(\gamma). \tag{51}$$

7. PROCEDURE ON HOW TO DETERMINE THE OPTIMAL THRESHOLD

7.1. Two Targets

What makes the scheme in this paper very useful in practical implementation of radar target recognition is that the optimal threshold $\gamma_{\mathrm{opt}}^{\mathrm{simul}}$ for practical implementation of Eq. (25) can be calculated analytically from $\gamma = \gamma_{\mathrm{opt}}^{\mathrm{simul}}$ using Eq. (28) or Eq. (29).

The procedure for getting the optimal threshold for two targets can be summarized as follows:

(i) Given σ^2 of $g_{n|k}$ in Eq. (1), calculate $\gamma_{\mathrm{opt}}^{\mathrm{analy}}$ from γ value satisfying Eq. (29) or γ value maximizing Eq. (28).

(ii) Use $\gamma = \gamma_{\mathrm{opt}}^{\mathrm{simul}} = \gamma_{\mathrm{opt}}^{\mathrm{analy}}$ in Eq. (25) to get the maximum probability of identification in practical implementation.

The procedure is essentially based on the fact that the simulation performance in Eq. (23), Eq. (24) and Eq. (25) do agree with the analytic performance in Eq. (26), Eq. (27) and Eq. (28) respectively, for all γ values in Eq. (31).

Accordingly, $\gamma = \gamma_{\text{opt}}^{\text{simul}}$ maximizing Eq. (25) can be found from $\gamma = \gamma_{\text{opt}}^{\text{analy}}$ maximizing Eq. (28) or $\gamma = \gamma_{\text{opt}}^{\text{analy}}$ satisfying Eq. (29).

Note that the PDF's and the CDF's in Eq. (28) and Eq. (29) can be analytically obtained, given the variance of σ^2 of $g_{n|k}$ in Eq. (1). We do not have to know specific realization of $g_{n|k}$ and $\mathbf{y}$ to get the PDF's and the CDF's in Eq. (28) and Eq. (29), from which we can get the optimum threshold $\gamma = \gamma_{\text{opt}}^{\text{analy}}$.

That is, we do not have to perform the Monte-Carlo simulation in Eq. (25) to get $\gamma = \gamma_{\text{opt}}^{\text{analy}}$. $\gamma = \gamma_{\text{opt}}^{\text{analy}}$ from Eq. (28) or Eq. (29) can be used in direct evaluation of Eq. (25) with $\gamma = \gamma_{\text{opt}}^{\text{simul}} = \gamma_{\text{opt}}^{\text{analy}}$ via the Monte-Carlo simulation.

7.2. Multiple Targets

For more than two targets, we can not calculate $P_I^{\text{analy}}(\gamma)$ analytically, and only get the upper bound $P_I^{\text{up}}(\gamma)$ and the lower bound $P_I^{\text{lo}}(\gamma)$ of the probability of classification [162]. The threshold values, at which $P_I^{\text{up}}(\gamma)$ and $P_I^{\text{lo}}(\gamma)$ are maximized, are denoted as $\gamma_{\text{opt}}^{\text{up}}$ in Eq. (51) and $\gamma_{\text{opt}}^{\text{lo}}$ in Eq. (50), respectively. We define $\gamma_{\text{opt}}^{\text{analy}}$ using $\gamma_{\text{opt}}^{\text{lo}}$ and $\gamma_{\text{opt}}^{\text{up}}$ as follows:

$$\gamma_{\text{opt}}^{\text{analy}} = \begin{cases} \gamma_{\text{opt}}^{\text{lo}}, & P_{I|1}^{\text{simul}}(\gamma_{\text{opt}}^{\text{lo}}) > P_{I|1}^{\text{simul}}(\gamma_{\text{opt}}^{\text{up}}) \\ \gamma_{\text{opt}}^{\text{up}}, & P_{I|1}^{\text{simul}}(\gamma_{\text{opt}}^{\text{lo}}) < P_{I|1}^{\text{simul}}(\gamma_{\text{opt}}^{\text{up}}) \end{cases} \tag{52}$$

where $\gamma_{\text{opt}}^{\text{lo}}$ and $\gamma_{\text{opt}}^{\text{up}}$ are obtained from Eq. (50) and Eq. (51), respectively.

Note that $\gamma_{\text{opt}}^{\text{lo}}$ and $\gamma_{\text{opt}}^{\text{up}}$ should be obtained for each signal-to-noise ratio (SNR), which results in different $\gamma_{\text{opt}}^{\text{analy}}$ for each SNR.

8. NUMERICAL RESULTS

We use two straight wires of length = 1.0 m and 1.2 m for two targets. For three targets, the three straight wires of length = 0.8 m, 1.0 m and 1.2 m are used.

When we only consider two targets, we compare the analytic results in Eq. (28) with the simulation-based performance. For multiple targets, the analytic results in Eq. (48) and Eq. (47) are compared

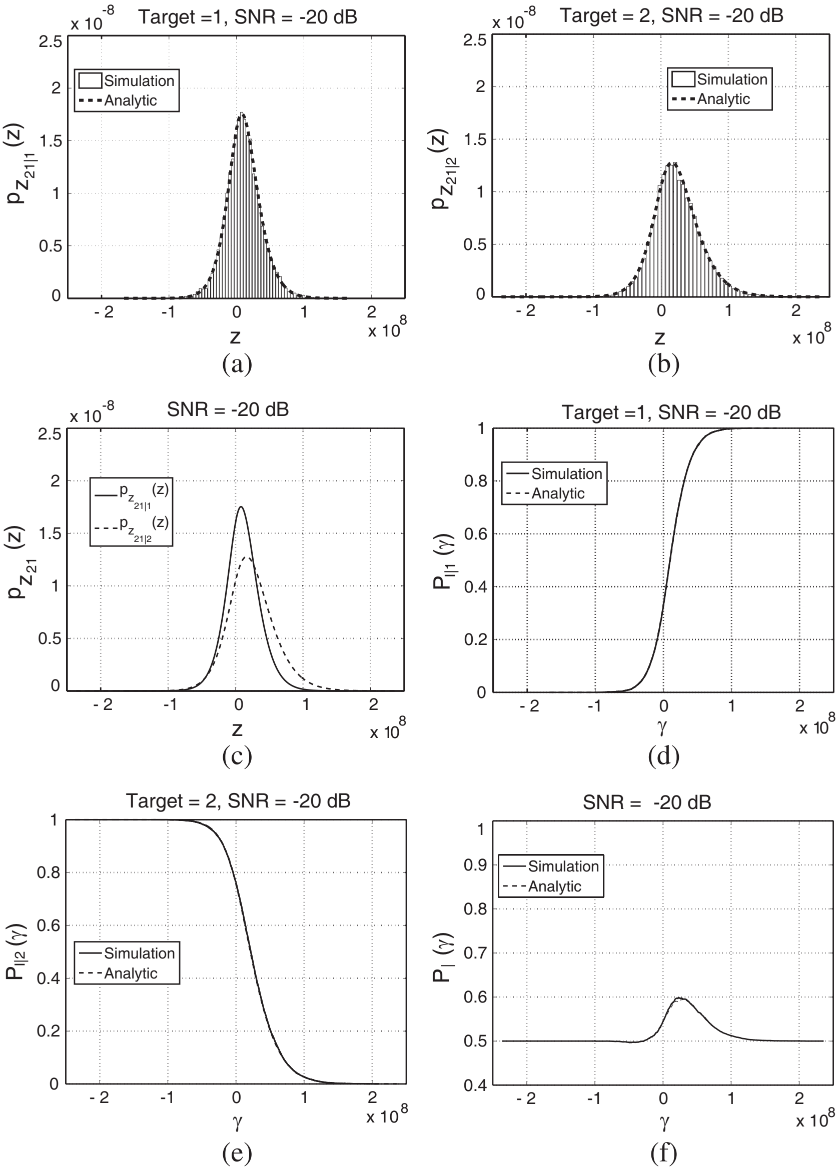

Figure 1. Dependence of $p_{Z_{21|1}}(z)$, $p_{Z_{21|2}}(z)$, $P_{I|1}(\gamma)$, $P_{I|2}(\gamma)$ and $P_I(\gamma)$ on the value of γ for two straight wires of length $= 1.0\,\mathrm{m}$ and $1.2\,\mathrm{m}$ (SNR $= -20\,\mathrm{dB}$).

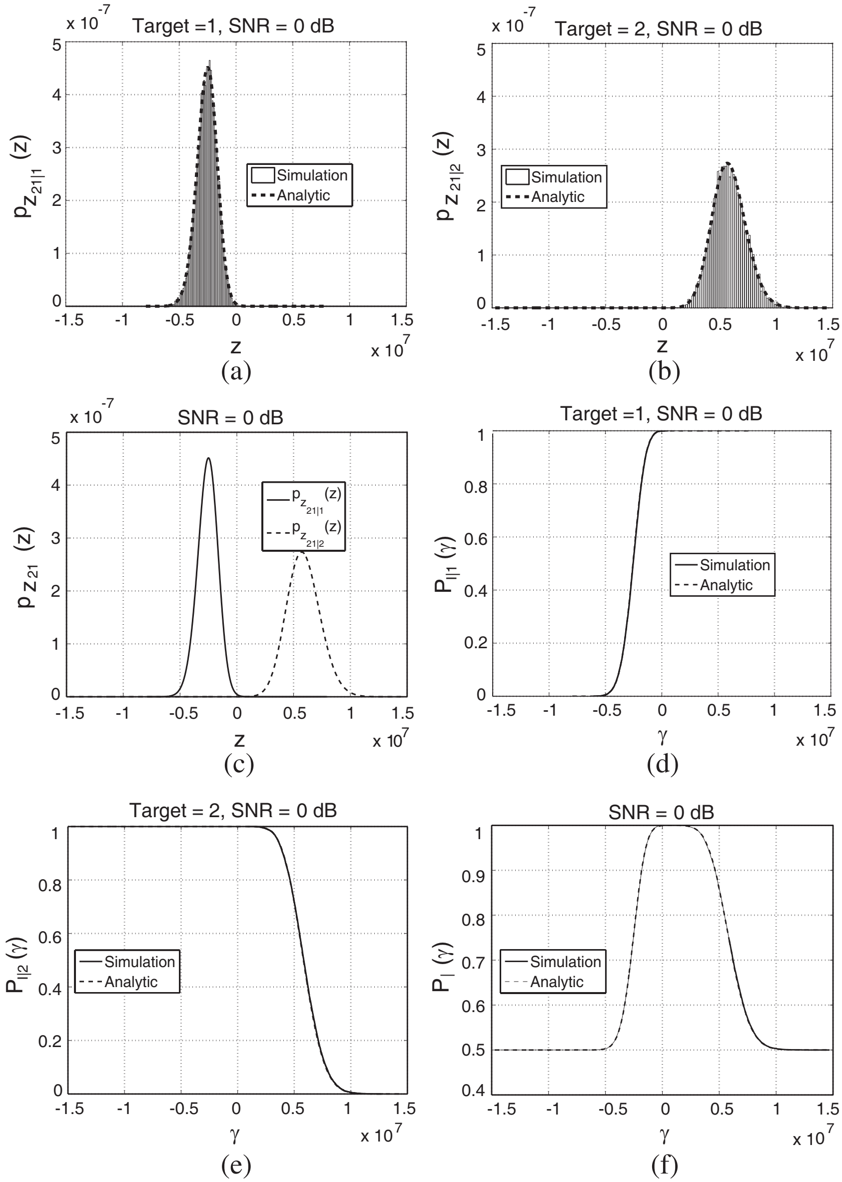

Figure 2. Dependence of $p_{Z_{21|1}}(z)$, $p_{Z_{21|2}}(z)$, $P_{I|1}(\gamma)$, $P_{I|2}(\gamma)$ and $P_I(\gamma)$ on the value of γ for two straight wires of length $= 1.0\,\mathrm{m}$ and $1.2\,\mathrm{m}$ (SNR $= 0\,\mathrm{dB}$).

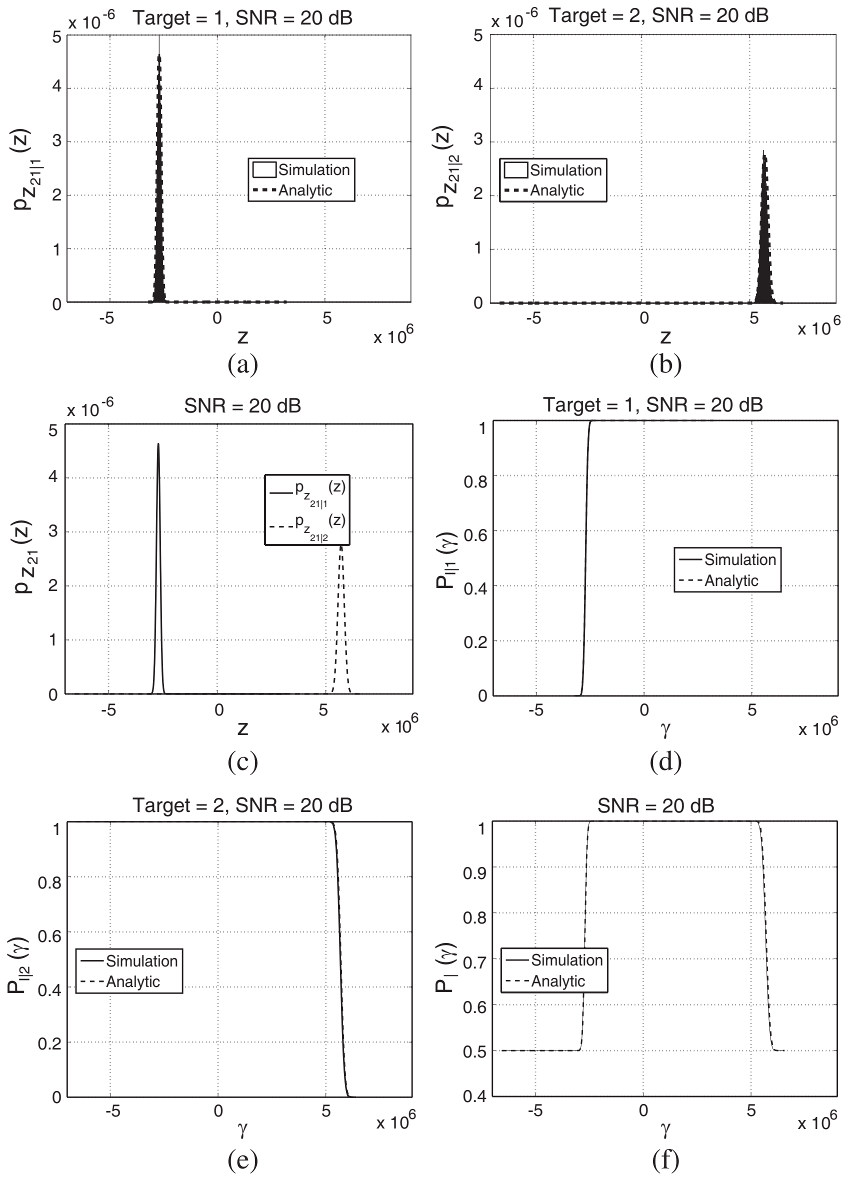

Figure 3. Dependence of $p_{Z_{21|1}}(z)$, $p_{Z_{21|2}}(z)$, $P_{I|1}(\gamma)$, $P_{I|2}(\gamma)$ and $P_I(\gamma)$ on the value of γ for two straight wires of length $= 1.0\,\mathrm{m}$ and $1.2\,\mathrm{m}$ ($\mathrm{SNR} = 20\,\mathrm{dB}$).

with the results based on the Monte-Carlo simulation. In getting the simulation-based performance, the probability of correct classification is obtained from 10,000 repetitions.

The noiseless frequency response is obtained via the method of moments (MoM). We calculated the back-scattered field. The frequency response up to 0.5 GHz is obtained in increments of 7.8 MHz. The incident angle for all the numerical examples is $\theta = 30°$. The frequency response is inverse Fourier transformed to obtain the time domain response.

The numbers of the natural frequencies for two targets

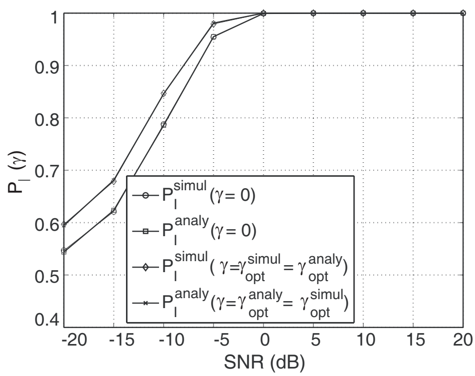

Figure 4. The performance improvement at $\gamma = \gamma_{\text{opt}}^{\text{analy}} = \gamma_{\text{opt}}^{\text{simul}}$ over the performance at $\gamma = 0$ for two straight wires of length = 1.0 m and 1.2 m.

Table 2. The optimal threshold values in Fig. 4 for various SNR values.

SNR (dB)	$\gamma_{\text{opt}}^{\text{analy}} = \gamma_{\text{opt}}^{\text{simul}}$
-20	2.97×10^7
-15	0.72×10^7
-10	0.25×10^7
-5	0.11×10^6
0	$-0.79 \times 10^6 < \gamma_{\text{opt}}^{\text{analy}} = \gamma_{\text{opt}}^{\text{simul}} < 2.95 \times 10^6$
5	$-1.66 \times 10^6 < \gamma_{\text{opt}}^{\text{analy}} = \gamma_{\text{opt}}^{\text{simul}} < 4.07 \times 10^6$
10	$-2.14 \times 10^6 < \gamma_{\text{opt}}^{\text{analy}} = \gamma_{\text{opt}}^{\text{simul}} < 4.74 \times 10^6$
15	$-2.39 \times 10^6 < \gamma_{\text{opt}}^{\text{analy}} = \gamma_{\text{opt}}^{\text{simul}} < 5.11 \times 10^6$
20	$-2.53 \times 10^6 < \gamma_{\text{opt}}^{\text{analy}} = \gamma_{\text{opt}}^{\text{simul}} < 5.35 \times 10^6$

corresponding to the frequency range up to 0.5 GHz are $M_1 = 6$ and $M_2 = 8$ [162].

In Figs. 1–3, we illustrate how $p_{Z_{21|1}}(z)$, $p_{Z_{21|2}}(z)$, $P_{I|1}(\gamma)$, $P_{I|2}(\gamma)$ and $P_I(\gamma)$ look for various SNR's.

In Figs. 1(a)–3(a) and Figs. 1(b)–3(b), we confirm that the analytic PDF's $p_{Z_{21|1}}(z)$ and $p_{Z_{21|2}}(z)$ agree quite well with the empirical PDF's obtained from the histogram using $Z_{21|1}$ values and $Z_{21|2}$ values in Eq. (8) from the Monte-Carlo simulation for each SNR value. Refer to Section 3 to see how to obtain the analytic PDF's of $p_{Z_{21|1}}(z)$ and $p_{Z_{21|2}}(z)$ [162].

In Figs. 1(c)–3(c), we overlap the analytic PDF's of $Z_{21|1}$ and $Z_{21|2}$ to graphically check at what γ value Eq. (29) holds. $P_{I|1}(\gamma)$ in Eq. (26), $P_{I|2}(\gamma)$ in Eq. (27) and $P_I(\gamma)$ in Eq. (28) are shown in Figs. 1(d)–3(d), Figs. 1(e)–3(e) and Figs. 1(f)–3(f), respectively. Note that γ values

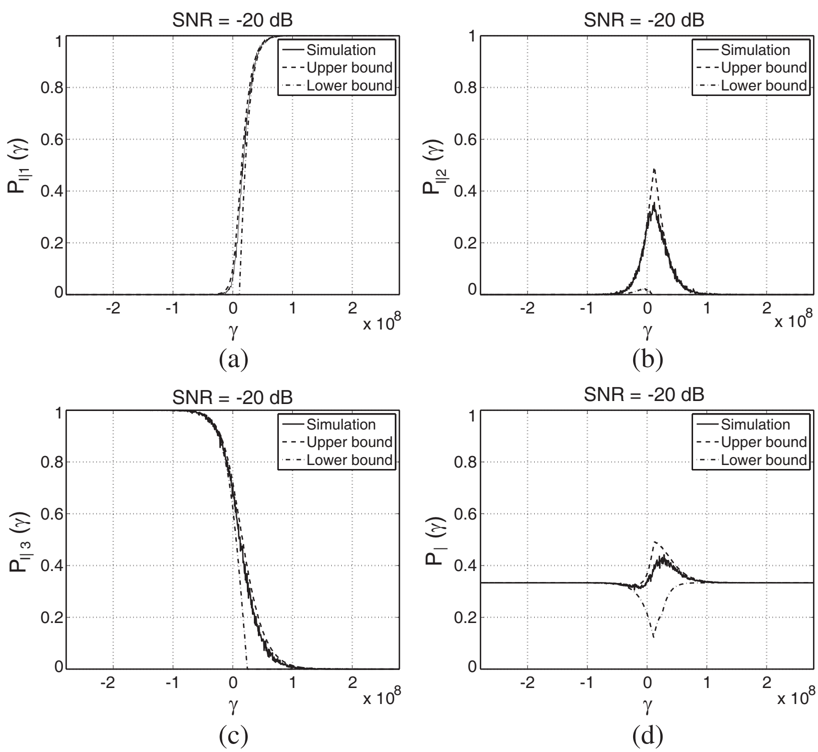

Figure 5. Analytical and simulated results as a function of γ value for three targets (SNR $= -20$ dB, $\gamma_{\text{opt}}^{\text{analy}} = 1.28 \times 10^7$, $\gamma_{\text{opt}}^{\text{simul}} = 2.84 \times 10^7$). (a) $P_{I|1}(\gamma)$, (b) $P_{I|2}(\gamma)$, (c) $P_{I|3}(\gamma)$ and (d) $P_I(\gamma)$.

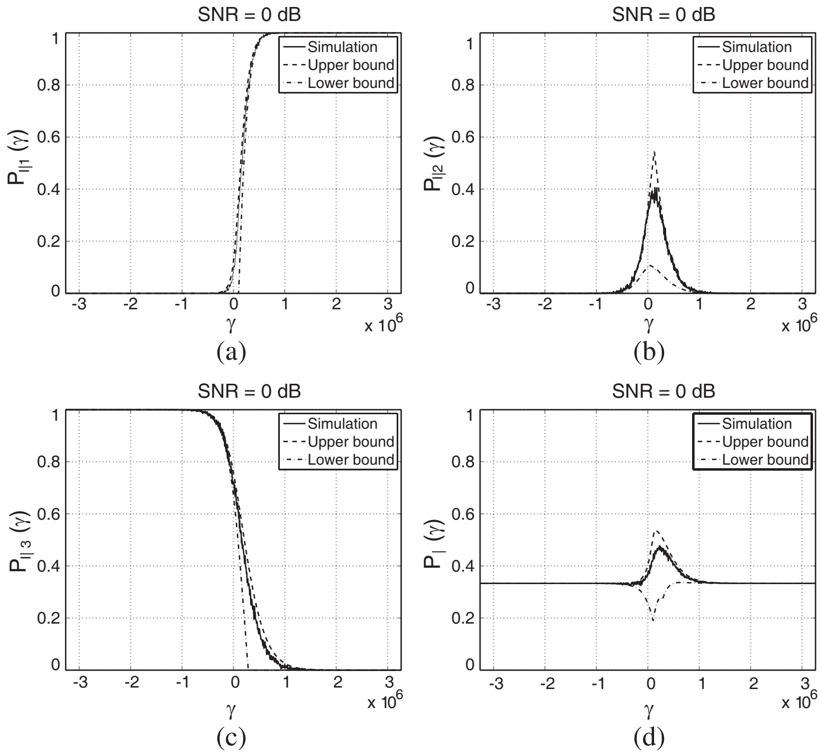

Figure 6. Analytical and simulated results as a function of γ value for three targets (SNR $= 0\,\mathrm{dB}$, $\gamma_{\mathrm{opt}}^{\mathrm{analy}} = 0.15 \times 10^6$, $\gamma_{\mathrm{opt}}^{\mathrm{simul}} = 0.22 \times 10^6$). (a) $P_{I|1}(\gamma)$, (b) $P_{I|2}(\gamma)$, (c) $P_{I|3}(\gamma)$ and (d) $P_I(\gamma)$.

maximizing Eq. (28) coincide with γ values satisfying Eq. (29) for all SNR's, which can be graphically checked by comparing γ value at which the PDF's of $Z_{21|1}$ and $Z_{21|2}$ in Figs. 1(c)–3(c) overlap with γ value at which $P_I(\gamma)$ is maximized in Figs. 1(f)–3(f). The optimal values of the thresholds are $\gamma_{\mathrm{opt}}^{\mathrm{anlay}} = 2.97 \times 10^7$, $-0.79 \times 10^6 < \gamma_{\mathrm{opt}}^{\mathrm{anlay}} < 2.95 \times 10^6$ and $-2.53 \times 10^6 < \gamma_{\mathrm{opt}}^{\mathrm{anlay}} < 5.35 \times 10^6$ for SNR $= -20\,\mathrm{dB}$, SNR $= 0\,\mathrm{dB}$, and SNR $= 20\,\mathrm{dB}$, respectively.

For SNR $= 0\,\mathrm{dB}$, since $p_{Z_{21|1}}(z)$ is almost zero for $z > -0.79 \times 10^6$, and $p_{Z_{21|2}}(z)$ is nearly zero for $z < 2.95 \times 10^6$, the probability of correct classification is nearly constant for the threshold value of $-0.79 \times 10^6 < \gamma < 2.95 \times 10^6$. Similarly, the optimal threshold for SNR $= 20\,\mathrm{dB}$ can be expressed as $-2.53 \times 10^6 < \gamma < 5.35 \times 10^6$.

It is also shown in Figs. 1(d)–3(d), Figs. 1(e)–3(e) and Figs. 1(f)–3(f) that analytic $P_{I|1}^{\mathrm{analy}}(\gamma)$, $P_{I|2}^{\mathrm{analy}}(\gamma)$ and $P_I^{\mathrm{analy}}(\gamma)$ show agreements with simulated $P_{I|1}^{\text{simul}}(\gamma)$, $P_{I|2}^{\text{simul}}(\gamma)$ and $P_{I}^{\text{simul}}(\gamma)$ for all γ values in Eq. (31).

In Fig. 4, we illustrate how much improvement we can get by adopting the optimal threshold $\gamma = \gamma_{\text{opt}}^{\text{analy}} = \gamma_{\text{opt}}^{\text{simul}}$ in comparison with $\gamma = 0$. In Table 2, the optimal threshold values are explicitly shown. Note that the $\gamma_{\text{opt}}^{\text{analy}}$ value should be calculated using Eq. (28) or Eq. (29) for each SNR value. Since we have more performance improvement at low SNR than high SNR, the proposed scheme is useful at low SNR. It is also shown that analytic performance shows an excellent agreement with simulation performance at $\gamma = \gamma_{\text{opt}}^{\text{analy}} = \gamma_{\text{opt}}^{\text{simul}}$ as well as at $\gamma = 0$.

In Figs. 5–7, we illustrate the results for three targets. The three targets are straight wires of length = 0.8 meter, 1.0 meter, and

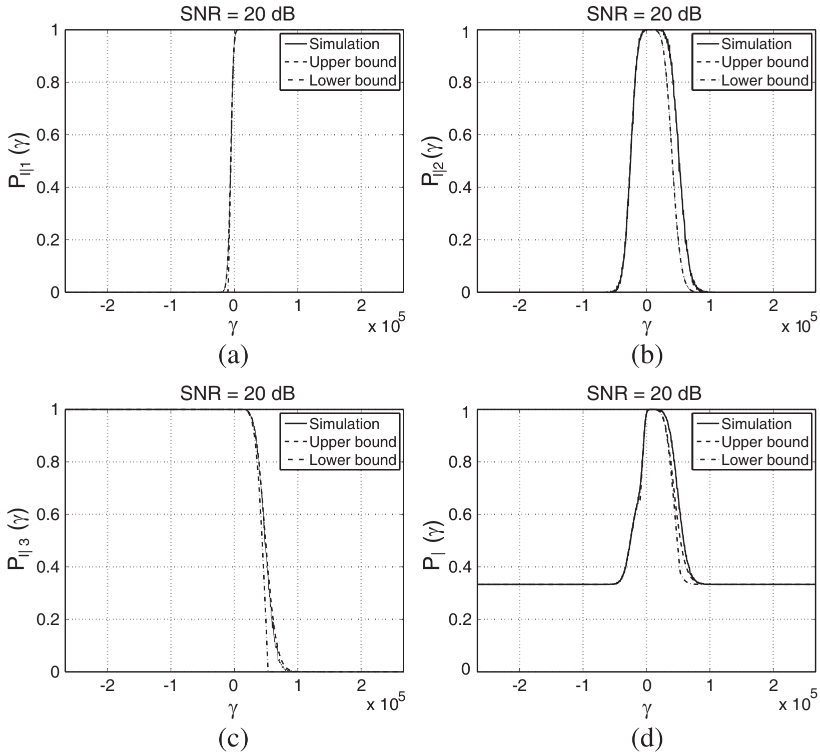

Figure 7. Analytical and simulated results as a function of γ value for three targets (SNR = 20 dB, $0.10 \times 10^4 < \gamma_{\text{opt}}^{\text{analy}} < 2.13 \times 10^4$, $0.10 \times 10^4 < \gamma_{\text{opt}}^{\text{simul}} < 2.08 \times 10^4$). (a) $P_{I|1}(\gamma)$, (b) $P_{I|2}(\gamma)$, (c) $P_{I|3}(\gamma)$ and (d) $P_I(\gamma)$.

1.2 meter with $M_1 = 4$, $M_2 = 6$ and $M_3 = 8$, respectively [162].

In Figs. 5–7(a), we show $P^{\text{simul}}_{I|1}(\gamma)$, $P^{\text{up}}_{I|1}(\gamma)$ and $P^{\text{lo}}_{I|1}(\gamma)$ as γ varies for various SNR values. Note that, in Figs. 5–7, the simulation performance is actually between the lower bound and the upper bound for all γ values:

$$P^{\text{lo}}_{I|k}(\gamma) \leq P^{\text{simul}}_{I|k}(\gamma) \leq P^{\text{up}}_{I|k}(\gamma). \tag{53}$$

Similarly, the results assuming that the true targets are target 2 and target 3 are shown in Figs. 5–7(b) and Figs. 5–7(c), respectively.

The results from Eq. (44) and Eq. (45) are used for an upper bound and a lower bound in Figs. 5–7(a), Figs. 5–7(b) and Figs. 5–7(c). The simulation performance in Figs. 5–7(a), Figs. 5–7(b) and Figs. 5–7(c)

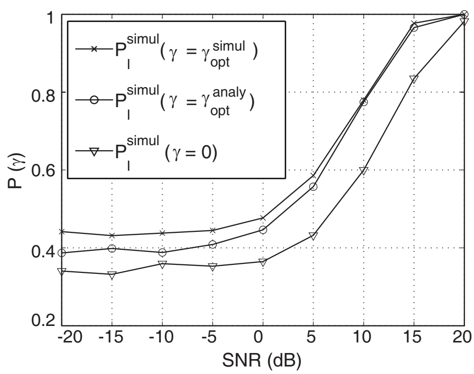

Figure 8. The performance improvement at $\gamma = \gamma^{\text{simul}}_{\text{opt}}$ and $\gamma = \gamma^{\text{analy}}_{\text{opt}}$ over the performance at $\gamma = 0$ for three straight wires of length = 0.8 m, 1.0 m and 1.2 m.

Table 3. The optimal threshold values for three targets.

SNR (dB)	$\gamma^{\text{anlay}}_{\text{opt}}$	$\gamma^{\text{simul}}_{\text{opt}}$
-20	1.28×10^7	2.84×10^7
-15	0.40×10^7	0.53×10^7
-10	0.12×10^7	0.21×10^7
-5	0.40×10^6	0.74×10^6
0	0.15×10^6	0.22×10^6
5	0.05×10^6	0.08×10^6
10	0.03×10^6	0.02×10^6
15	0.01×10^6	0.01×10^6
20	$0.10 \times 10^4 < \gamma^{\text{anlay}}_{\text{opt}} < 2.13 \times 10^4$	$0.10 \times 10^4 < \gamma^{\text{simul}}_{\text{opt}} < 2.08 \times 10^4$

Table 4. The performance improvement at $\gamma = \gamma_{\text{opt}}^{\text{simul}}$ and $\gamma = \gamma_{\text{opt}}^{\text{analy}}$ over the performance at $\gamma = 0$ for three straight wires of length = 0.8 m, 1.0 m and 1.2 m (Numerical values).

SNR (dB)	−20	−15	−10	−5	0	5	10	15	20
P_I^{simul} $(\gamma = \gamma_{\text{opt}}^{\text{simul}})$	0.44	0.43	0.43	0.44	0.47	0.58	0.77	0.97	1.00
P_I^{simul} $(\gamma = \gamma_{\text{opt}}^{\text{analy}})$	0.38	0.39	0.38	0.40	0.44	0.55	0.77	0.96	1.00
P_I^{simul} $(\gamma = 0)$	0.34	0.33	0.35	0.35	0.36	0.43	0.60	0.83	0.98

are obtained from Eq. (46).

The upper bound and the lower bound in Figs. 5–7(d) are obtained from Eq. (47) and Eq. (48). The simulation performance in Figs. 5–7(d) are from Eq. (49). $\gamma_{\text{opt}}^{\text{analy}}$ and $\gamma_{\text{opt}}^{\text{simul}}$ values are also specified in the captions of Figs. 5–7.

In Fig. 8, we illustrate $P_I^{\text{simul}}(\gamma = 0)$, $P_I^{\text{simul}}(\gamma = \gamma_{\text{opt}}^{\text{simul}})$ and $P_I^{\text{simul}}(\gamma = \gamma_{\text{opt}}^{\text{analy}})$ for various SNR values. In Table 3, we also tabulate $P_I^{\text{simul}}(\gamma = \gamma_{\text{opt}}^{\text{simul}})$, $P_I^{\text{simul}}(\gamma = \gamma_{\text{opt}}^{\text{analy}})$, and $P_I^{\text{simul}}(\gamma = 0)$ in Fig. 8.

Although we get $\gamma_{\text{opt}}^{\text{lo}}$ and $\gamma_{\text{opt}}^{\text{up}}$ from Eq. (50) and Eq. (51), respectively, using the PDF's and the CDF's without the Monte-Carlo simulation, we can not get $\gamma_{\text{opt}}^{\text{simul}}$ analytically. We do have to perform the Monte-Carlo simulation as γ value varies to see what γ value results in the maximum $P_I^{\text{simul}}(\gamma)$.

How to choose the sub-optimal threshold without exhaustive search over γ value is given in Eq. (50)–Eq. (52). $\gamma_{\text{opt}}^{\text{analy}}$ and $\gamma_{\text{opt}}^{\text{simul}}$ values in Fig. 8 are indicated in Table 4. In Fig. 8, we illustrate how close $P_I^{\text{simul}}(\gamma = \gamma_{\text{opt}}^{\text{analy}})$ is to $P_I^{\text{simul}}(\gamma = \gamma_{\text{opt}}^{\text{simul}})$, and how much $P_I^{\text{simul}}(\gamma = \gamma_{\text{opt}}^{\text{analy}})$ has improved in comparison with $P_I^{\text{simul}}(\gamma = 0)$.

9. CONCLUSIONS

We considered the dependence of the probability of correct identification on the value of the threshold in the radar target recognition using the natural frequency. We illustrated how to determine the optimum threshold for use with the natural frequency-based radar target recognition of two targets. For multiple targets, we show how to determine the sub-optimal threshold.

We extended the formulation in [162] by adopting a nonzero threshold. How the probability of correct identification is dependent on the threshold value is addressed by numerical evaluation of the PDF.

The derivation is validated by comparing the analytical performance with the performance based on the Monte-Carlo simulation. To show the agreement between the analytic results and the simulation results for nonzero threshold value, the late time responses of simple targets are used. The results for two targets show that the scheme presented in this paper can be used to determine the optimum threshold for use with the performance analysis of the natural frequency-based radar target recognition in the time domain. For more than two targets, we show how to choose the threshold which is very close to the optimum threshold.

ACKNOWLEDGMENT

This research was supported by Basic Science Research Program through the National Research Foundation of Korea (NRF) funded by the Ministry of Education, Science and Technology (2012-0002347).

REFERENCES

1. Chen, J., S. Quegan, and X. Yin, "Calibration of spaceborne linearly polarized low frequency SAR using polarimetric selective radar calibrators," *Progress In Electromagnetics Research*, Vol. 114, 89–111, 2011.
2. Li, S., Y. Tian, G. Lu, Y. Zhang, H. J. Xue, J.-Q. Wang, and X.-J. Jing, "A new kind of non-acoustic speech acquisition method based on millimeter wave radar," *Progress In Electromagnetics Research*, Vol. 130, 17–40, 2012.
3. Alvarez-Lopez, Y., C. Garcia-Gonzalez, C. Vazquez-Antuna, S. Ver-Hoeye, and F. Las-Heras, "Frequency scanning based radar system," *Progress In Electromagnetics Research*, Vol. 132, 275–296, 2012.
4. Li, S., Y. Tian, G. Lu, Y. Zhang, H. J. Xue, J.-Q. Wang, and X.-J. Jing, "A new kind of non-acoustic speech acquisition method based on millimeter wave radar," *Progress In Electromagnetics Research*, Vol. 130, 17–40, 2012.
5. Alejos, A. V., M. Dawood, and M. Garcia Snchez, "Extended optimal filters for adaptive-ontransmit radar systems using binary codes," *Progress In Electromagnetics Research*, Vol. 130, 41–66, 2012.

6. Albert, M. D., Y. J. Lee, H.-T. Ewe, and H.-T. Chuah, "Multilayer model formulation and analysis of radar backscattering from sea ice," *Progress In Electromagnetics Research*, Vol. 128, 267–290, 2012.
7. Liu, Z., X. Wei, and X. Li, "Adaptive clutter suppression for airborne random pulse repetition interval radar based on compressed sensing," *Progress In Electromagnetics Research*, Vol. 128, 291–311, 2012.
8. Li, Y., X. Jing, H. Lv, and J. Wang, "Analysis of characteristics of two close stationary human targets detected by impulse radio UWB radar," *Progress In Electromagnetics Research*, Vol. 126, 429–447, 2012.
9. Zhang, J.-P., Z.-S. Wu, Y.-S. Zhang, and B. Wang, "A four-parameter M-profile model for the evaporation duct estimation from radar clutter," *Progress In Electromagnetics Research*, Vol. 126, 555–571, 2012.
10. Peng, X., W. Tan, Y. Wang, W. Hong, and Y. Wu, "Convolution back-projection imaging algorithm for downward-looking sparse linear array three dimensional synthetic aperture radar," *Progress In Electromagnetics Research*, Vol. 129, 287–313, 2012.
11. Dusseaux, R., E. Vannier, O. Taconet, and G. Granet, "Study of backscatter signature for seedbed surface evolution under rainfall — Influence of radar precision," *Progress In Electromagnetics Research*, Vol. 125, 415–437, 2012.
12. Jeong, S.-H., H.-Y. Yu, J.-E. Lee, J.-N. Oh, and K.-H. Lee, "A multi-beam and multi-range radar with FMCW and digital beam forming for automotive applications," *Progress In Electromagnetics Research*, Vol. 124, 285–299, 2012.
13. Kirkland, D. M., "An alternative range migration correction algorithm for focusing moving targets," *Progress In Electromagnetics Research*, Vol. 131, 227–241, 2012.
14. Niu, X., Z.-P. Nie, and S. He, "The application of modified phase extracted basis functions in scattering analysis of dielectric-coated targets," *Progress In Electromagnetics Research*, Vol. 127, 121–137, 2012.
15. Wu, J., Z. Li, Y. Huang, Q. H. Liu, and J. Yang, "Processing one-stationary bistatic SAR data using inverse scaled Fourier transform," *Progress In Electromagnetics Research*, Vol. 129, 143–159, 2012.
16. Liu, Y., Y.-K. Deng, R. Wang, and X. Jia, "Bistatic FMCW SAR raw signal simulator for extended scenes," *Progress In Electromagnetics Research*, Vol. 128, 479–502, 2012.

17. Hong, S., L. Wang, Z.-G. Shi, and K. S. Chen, "Simplified particle PHD filter for multiple-target tracking: Algorithm and architecture," *Progress In Electromagnetics Research*, Vol. 119, 35–57, 2011.
18. Riaz, M. M. and A. Ghafoor, "Information theoretic criterion based clutter reduction for ground penetrating radar," *Progress In Electromagnetics Research B*, Vol. 45, 147–164, 2012.
19. Del Corte Valiente, A., "Evaluation of a non-cooperative aircraft surveillance system based on short range continuous-wave radars," *Progress In Electromagnetics Research B*, Vol. 43, 1–18, 2012.
20. Vaitilingom, L. and A. Khenchaf, "Radar cross sections of sea and ground clutter estimated by two scale model and small slope approximation in HF-VHF bands," *Progress In Electromagnetics Research B*, Vol. 29, 311–338, 2011.
21. Thajudeen, C., A. Hoorfar, F. Ahmad, and T. Dogaru, "Measured complex permittivity of walls with different hydration levels and the effect on power estimation of TWRI target returns," *Progress In Electromagnetics Research B*, Vol. 30, 177–199, 2011.
22. Liu, Q., S. Xing, X. Wang, J. Dong, and D. Dai, "A strip-map SAR coherent jammer structure utilizing periodic modulation technology," *Progress In Electromagnetics Research B*, Vol. 28, 111–128, 2011.
23. Catapano, I., F. Soldovieri, and L. Crocco,"On the feasibility of the linear sampling method for 3D GPR surveys," *Progress In Electromagnetics Research*, Vol. 118, 185–203, 2011.
24. Alvarez-Lopez, Y., C. Garcia-Gonzalez, C. Vazquez-Antuna, S. Ver-Hoeye, and F. Las-Heras, "Frequency scanning based radar system," *Progress In Electromagnetics Research*, Vol. 132, 275–296, 2012.
25. Zakeri, B. G., M. R. Zahabi, and S. Alighale, "Sidelobes level improvement by using a new scheme used in microwave pulse compression radars," *Progress In Electromagnetics Research Letters*, Vol. 30, 81–90, 2012.
26. Tian, B., D.-Y. Zhu, and Z.-D. Zhu, "A novel moving target detection approach for dual-channel SAR system," *Progress In Electromagnetics Research*, Vol. 115, 191–206, 2011.
27. Budillon, A., A. Evangelista, and G. Schirinzi, "GLRT detection of moving targets via multibaseline along-track interferometric SAR systems," *IEEE Geoscience and Remote Sensing Letters*, Vol. 9, 348–352, 2012.
28. Guan, J., X.-L. Chen, Y. Huang, and Y. He, "Adaptive fractional

Fourier transform-based detection algorithm for moving target in heavy sea clutter," *IET Radar, Sonar and Navigation*, Vol. 6, 389–401, 2012.

29. Ray, P. and P. K. Varshney, "Radar target detection framework based on false discovery rate," *IEEE Transactions on Aerospace and Electronic Systems*, Vol. 47, 1277–1292, 2011.
30. Zhou, S. H. and H. W. Liu, "Signal fusion-based target detection algorithm for spatial diversity radar," *IET Radar, Sonar and Navigation*, Vol. 5, 204–214, 2011.
31. Debes, C., A. M. Zoubir, and M. G. Amin, "Enhanced detection using target polarization signatures in through-the-wall radar imaging," *IEEE Transactions on Geoscience and Remote Sensing*, Vol. 50, 1968–1979, 2012.
32. Liu, B. and W. Chang, "A novel range-spread target detection approach for frequency stepped chirp radar," *Progress In Electromagnetics Research*, Vol. 131, 275–292, 2012.
33. Mohammadpoor, M., R. S. A. Raja Abdullah, A. Ismail, and A. F. Abas, "A circular synthetic aperture radar for on-the-ground object detection," *Progress In Electromagnetics Research*, Vol. 122, 269–292, 2012.
34. Hao, C., F. Bandiera, J. Yang, D. Orlando, S. Yan, and C. Hou, "Adaptive detection of multiple point-like targets under conic constraints," *Progress In Electromagnetics Research*, Vol. 129, 231–250, 2012.
35. Tugac, S. and M. Efe, "Radar target detection using hidden markov models," *Progress In Electromagnetics Research B*, Vol. 44, 241–259, 2012.
36. Chen, S., L. Kong, and J. Yang, "Small target detection in heavy sea clutter," *Progress In Electromagnetics Research B*, Vol. 44, 405–425, 2012.
37. Wang, J.-T., H.-Q. Wang, Y.-L. Qin, and Z. Zhuang, "Efficient adaptive detection threshold optimization for tracking maneuvering targets in clutter," *Progress In Electromagnetics Research B*, Vol. 41, 357–375, 2012.
38. Magaz, B., A. Belouchrani, and M. Hamadouche, "Automatic threshold selection in OS-CFAR radar detection using information theoretic criteria," *Progress In Electromagnetics Research B*, Vol. 30, 157–175, 2011.
39. Magaz, B., A. Belouchrani, and M. Hamadouche, "A new adaptive linear combined CFAR detector in presence of interfering targets," *Progress In Electromagnetics Research B*, Vol. 34, 367–387, 2011.

40. Wang, F.-F. and Y.-R. Zhang, "The support vector machine for dielectric target detection through a wall," *Progress In Electromagnetics Research Letters*, Vol. 23, 119–128, 2011.
41. Conceicao, R. C., M. O'Halloran, M. Glavin, and E. Jones, "Numerical modelling for ultra wideband radar breast cancer detection and classification," *Progress In Electromagnetics Research B*, Vol. 34, 145–171, 2011.
42. Hatam, M., A. Sheikhi, and M. A. Masnadi-Shirazi, "Target detection in pulse-train MIMO radars applying ICA algorithms," *Progress In Electromagnetics Research*, Vol. 122, 413–435, 2012.
43. Zhou, W., J.-T. Wang, H. W. Chen, and X. Li, "Signal model and moving target detection based on MIMO synthetic aperture radar," *Progress In Electromagnetics Research*, Vol. 131, 311–329, 2012.
44. Yang, M. and G. Zhang, "Unsupervised target detection in SAR images using scattering center model and mean shift clustering algorithm," *Progress In Electromagnetics Research Letters*, Vol. 35, 11–18, 2012.
45. Le Marshall, N. W. D. and A. Z. Tirkel, "MIMO radar array for termite detection and imaging," *Progress In Electromagnetics Research B*, Vol. 28, 75–94, 2011.
46. Zhang, H., S. Y. Tan, and H. S. Tan, "Experimental study on a flanged parallel-plate dielectric waveguide probe for detection of buried inclusions," *Progress In Electromagnetics Research*, Vol. 111, 91–104, 2011.
47. Wang, X., J.-F. Chen, Z.-G. Shi, and K. S. Chen, "Fuzzy-control-based particle filter for maneuvering target tracking," *Progress In Electromagnetics Research*, Vol. 118, 1–15, 2011.
48. Wang, Q., J. Li, M. Zhang, and C. Yang, "H-infinity filter based particle filter for maneuvering target tracking," *Progress In Electromagnetics Research B*, Vol. 30, 103–116, 2011.
49. Diao, W.-H., X. Mao, H.-C. Zheng, Y.-L. Xue, and V. Gui, "Image sequence measures for automatic target tracking," *Progress In Electromagnetics Research*, Vol. 130, 447–472, 2012.
50. Sjogren, T. K., V. T. Vu, M. I. Pettersson, A. Gustavsson, and L. M. H. Ulander, "Moving target relative speed estimation and refocusing in synthetic aperture radar images," *IEEE Transactions on Aerospace and Electronic Systems*, Vol. 48, 2426–2436, 2012.
51. Hassanien, A., S. A. Vorobyov, and A. B. Gershman, "Moving target parameters estimation in noncoherent MIMO radar

systems," *IEEE Transactions on Signal Processing*, Vol. 60, 2354–2361, 2012.
52. Garcia-Donoro, D., I. Martinez-Fernandez, L. E. Garcia-Castillo, Y. Zhang, and T. K. Sarkar, "RCS computation using a parallel in-core and out-of-core direct solver," *Progress In Electromagnetics Research*, Vol. 118, 505–525, 2011.
53. Xu, H.-Y., H. Zhang, K. Lu, and X.-F. Zeng, "A holly-leaf-shaped monopole antenna with low RCS for UWB application," *Progress In Electromagnetics Research*, Vol. 117, 35–50, 2011.
54. De Cos, M. E., Y. Alvarez Lopez, and F. Las-Heras, "On the influence of coupling AMC resonances for RCS reduction in the SHF band," *Progress In Electromagnetics Research*, Vol. 117, 103–119, 2011.
55. Bennani, Y., F. Comblet, and A. Khenchaf, "RCS of complex targets: Original representation validated by measurements application to ISAR imagery," *IEEE Transactions on Geoscience and Remote Sensing*, Vol. 50, 3882–3891, 2012.
56. Shang, Y., S.-Q. Xiao, J.-L. Li, and B.-Z. Wang, "An electronically controllable method for radar cross section reduction for a microstrip antenna," *Progress In Electromagnetics Research*, Vol. 127, 15–30, 2012.
57. Zhu, X., W. Shao, J.-L. Li, and Y.-L. Dong, "Design and optimization of low RCS patch antennas based on a genetic algorithm," *Progress In Electromagnetics Research*, Vol. 122, 327–339, 2012.
58. Park, H.-G., K. K. Park, H.-T. Kim, and K.-T. Kim, "Improvement of RCS prediction using modified angular division algorithm," *Progress In Electromagnetics Research*, Vol. 123, 105–121, 2012.
59. Sirenko, K., V. Pazynin, Y. K. Sirenko, and H. Baci, "Compression and radiation of high-power short RF pulses. II. A novel antenna array design with combined compressor/radiator elements," *Progress In Electromagnetics Research*, Vol. 116, 271–296, 2011.
60. Li, J., B. Wei, Q. He, L.-X. Guo, and D.-B. Ge, "Time-domain iterative physical optics method for analysis of EM scattering from the target half buried in rough surface: PEC case," *Progress In Electromagnetics Research*, Vol. 121, 391–408, 2011.
61. Jandieri, V., K. Yasumoto, and Y.-K. Cho, "Rigorous analysis of electromagnetic scattering by cylindrical EBG structures," *Progress In Electromagnetics Research*, Vol. 121, 317–342, 2011.

62. Lin, G.-R., F.-S. Meng, and Y.-H. Lin, "Second-order scattering induced reflection divergence and nonlinear depolarization on randomly corrugated semiconductor nano-pillars," *Progress In Electromagnetics Research*, Vol. 117, 67–81, 2011.
63. Cui, Z., Y. Han, C. Y. Li, and W. Zhao, "Efficient analysis of scattering from multiple 3-D cavities by means of a FE-BI-DDM method," *Progress In Electromagnetics Research*, Vol. 116, 425–439, 2011.
64. Jiang, W.-Q., M. Zhang, H. Chen, and Y.-G. Lu, "CUDA implementation in the EM scattering of a three-layer canopy," *Progress In Electromagnetics Research*, Vol. 116, 457–473, 2011.
65. Du, Y., W.-Z. Yan, J.-C. Shi, Z. Li, and E.-X. Chen, "Electromagnetic scattering from a corn canopy at L and C bands," *Progress In Electromagnetics Research*, Vol. 114, 33–49, 2011.
66. Xiao, K., F. Zhao, S.-L. Chai, J.-J. Mao, and J. L.-W. Li, "Scattering analysis of periodic arrays using combined CBF/P-FFT method," *Progress In Electromagnetics Research*, Vol. 115, 131–146, 2011.
67. Zhu, X., Z. Zhao, W. Yang, Y. Zhang, Z.-P. Nie, and Q. H. Liu, "Iterative time-reversal mirror method for imaging the buried object beneath rough ground surface," *Progress In Electromagnetics Research*, Vol. 117, 19–33, 2011.
68. Qi, C., Z. Zhao, W. Yang, Z.-P. Nie, and G. Chen, "Electromagnetic scattering and Doppler analysis of three-dimensional breaking wave crests at low-grazing angles," *Progress In Electromagnetics Research*, Vol. 119, 239–252, 2011.
69. Valagiannopoulos, C. A., "Electromagnetic scattering of the field of a metamaterial slab antenna by an arbitrarily positioned cluster of metallic cylinders," *Progress In Electromagnetics Research*, Vol. 114, 51–66, 2011.
70. Chang, Y.-L., C.-Y. Chiang, and K.-S. Chen, "SAR image simulation with application to target recognition," *Progress In Electromagnetics Research*, Vol. 119, 35–57, 2011.
71. Lui, H.-S. and N. V. Shuley, "Resonance based target recognition using ultrawideband polarimetric signatures," *IEEE Transactions on Antennas and Propagation*, Vol. 60, 3985–3988, 2012.
72. Du, L., H. Liu, P. Wang, B. Feng, M. Pan, and Z. Bao, "Noise robust radar HRRP target recognition based on multitask factor analysis with small training data size," *IEEE Transactions on Signal Processing*, Vol. 60, 3546–3559, 2012.

73. Smith, G. E. and B. G. Mobasseri, "Robust through-the-wall radar image classification using a target-model alignment procedure," *IEEE Transactions on Image Processing*, Vol. 21, 754–767, 2012.
74. Zhang, H., N. M. Nasrabadi, Y. Zhang, and T. S. Huang, "Multi-view automatic target recognition using joint sparse representation," *IEEE Transactions on Aerospace and Electronic Systems*, Vol. 48, 2481–2497, 2012.
75. Du, L., H. Liu, Z. Bao, and M. Xing, "Radar HRRP target recognition based on higher order spectra," *IEEE Transactions on Signal Processing*, Vol. 53, 2359–2368, 2005.
76. Du, L., H. Liu, P. Wang, B. Feng, M. Pan, and Z. Bao, "Noise robust radar HRRP target recognition based on multitask factor analysis with small training data size," *IEEE Transactions on Signal Processing*, Vol. 60, 3546–3559, 2012.
77. Park, S.-H., J.-H. Lee, and K.-T. Kim, "Performance analysis of the scenario-based construction method for real target ISAR recognition," *Progress In Electromagnetics Research*, Vol. 128, 137–151, 2012.
78. Li, Q. and W. Xie, "Target classification with low-resolution surveillance radars based on multifractal features," *Progress In Electromagnetics Research B*, Vol. 45, 291–308, 2012.
79. Mishra, P., D. Singh, and Y. Yamaguchi, "Land cover classification of PALSAR images by knowledge based decision tree classifier and supervised classifiers based on SAR observables," *Progress In Electromagnetics Research B*, Vol. 30, 47–70, 2011.
80. Du, L., P. Wang, H. Liu, M. Pan, F. Chen, and Z. Bao, "Bayesian spatiotemporal multitask learning for radar HRRP target recognition," *IEEE Transactions on Signal Processing*, Vol. 59, 3182–3196, 2011.
81. Jia, Y., L. Kong, and X. Yang, "A novel approach to target localization through unknown walls for through-the-wall radar imaging," *Progress In Electromagnetics Research*, Vol. 119, 107–132, 2011.
82. Diao, W.-H., X. Mao, and V. Gui, "Metrics for performance evaluation of preprocessing algorithms in infrared small target images," *Progress In Electromagnetics Research*, Vol. 115, 35–53, 2011.
83. Zhang, M., Y. W. Zhao, H. Chen, and W.-Q. Jiang, "SAR imaging simulation for composite model of ship on dynamic ocean scene," *Progress In Electromagnetics Research*, Vol. 113, 395–412, 2011.

84. Xu, W., P. Huang, and Y.-K. Deng, "MIMO-TOPS mode for high-resolution ultra-wide-swath full polarimetric imaging," *Progress In Electromagnetics Research*, Vol. 121, 19–37, 2011.
85. Huang, Y., P. V. Brennan, D. Patrick, I. Weller, P. Roberts, and K. Hughes, "FMCW based MIMO imaging radar for maritime navigation," *Progress In Electromagnetics Research*, Vol. 115, 327–342, 2011.
86. Qi, Y., W. Tan, Y. Wang, W. Hong, and Y. Wu, "3D bistatic Omega-K imaging algorithm for near range microwave imaging systems with bistatic planar scanning geometry," *Progress In Electromagnetics Research*, Vol. 121, 409–431, 2011.
87. Xin, Y. H., Y. Z. Xiao, and J. C. Tie, "Fast 3D-ISAR image simulation of targets at arbitrary aspect angles through nonuniform fast Fourier transform (NUFFT)," *IEEE Transactions on Antennas and Propagation*, Vol. 60, 2597–2602, 2012.
88. Zhang L., Z.-J. Qiao, M.-D. Xing, J.-L. Sheng, R. Guo, and Z. Bao, "High-resolution ISAR imaging by exploiting sparse apertures," *IEEE Transactions on Antennas and Propagation*, Vol. 60, 997–1008, 2012.
89. Abe, Y., S. Kidera, and T. Kirimoto, "Accurate and omnidirectional UWB radar imaging algorithm with RPM method extended to curvilinear scanning model," *IEEE Geoscience and Remote Sensing Letters*, Vol. 9, 144–148, 2012.
90. Calvo-Gallego, J. and F. Prez-Martnez, "Simple traffic surveillance system based on range-doppler radar images," *Progress In Electromagnetics Research*, Vol. 125, 343–364, 2012.
91. Koo, V. C., Y. K. Chan, V. Gobi, M. Y. Chua, C. H. Lim, C.-S. Lim, C. C. Thum, T. S. Lim, Z. bin Ahmad, K. A. Mahmood, M. H. Bin Shahid, C. Y. Ang, W. Q. Tan, P. N. Tan, K. S. Yee, W. G. Cheaw, H. S. Boey, A. L. Choo, and B. C. Sew, "A new unmanned aerial vehicle synthetic aperture radar for environmental monitoring," *Progress In Electromagnetics Research*, Vol. 122, 245–268, 2012.
92. Felguera-Martin, D., J.-T. Gonzalez-Partida, and M. Burgos-Garcia, "Interferometric ISAR imaging on maritime target applications: Simulation of realistic targets and dynamics," *Progress In Electromagnetics Research*, Vol. 132, 571–586, 2012.
93. Yu, L. and Y. Zhang, "A 3D target imaging algorithm based on two-pass circular SAR observations," *Progress In Electromagnetics Research*, Vol. 122, 341–360, 2012.
94. Park, S.-H., J.-I. Park, and K.-T. Kim, "Motion compensation for squint mode spotlight SAR imaging using efficient 2D

interpolation," *Progress In Electromagnetics Research*, Vol. 128, 503–518, 2012.
95. Ji, W.-J. and C.-M. Tong, "Radar image of one dimension rough surface with buried object," *Progress In Electromagnetics Research B*, Vol. 36, 323–336, 2012.
96. Zhu, G. K. and M. Popovic, "Comparison of radar and thermoacoustic technique in microwave breast imaging," *Progress In Electromagnetics Research B*, Vol. 35, 1–14, 2011.
97. Desrumaux, L., M. Lalande, J. Andrieu, V. Bertrand, and B. Jecko, "An innovative radar imaging system based on the capability of an UWB array to steer successively in different directions," *Progress In Electromagnetics Research B*, Vol. 32, 91–106, 2011.
98. Zhang, W. and A. Hoorfar, "Two-dimensional diffraction tomographic algorithm for through-the-wall radar imaging," *Progress In Electromagnetics Research B*, Vol. 31, 205–218, 2011.
99. Gu, X. and Y. Zhang, "Resolution threshold analysis of music algorithm in radar range imaging," *Progress In Electromagnetics Research B*, Vol. 31, 297–321, 2011.
100. Buddendick, H. and T. F. Eibert, "Bistatic image formation from shooting and bouncing rays simulated current distributions," *Progress In Electromagnetics Research*, Vol. 119, 1–18, 2011.
101. Zhai, W. and Y. Zhang, "Application of super-SVA to stepped-chirp radar imaging with frequency band gaps between subchirps," *Progress In Electromagnetics Research B*, Vol. 30, 71–82, 2011.
102. Ikeuchi, R., K. H. Chan, and A. Hirata, "SAR and radiation characteristics of a dipole antenna above different finite EBG substrates in the presence of a realistichead model in the 3.5 GHz band," *Progress In Electromagnetics Research B*, Vol. 44, 53–70, 2012.
103. Ren, X.-Z., Y. F. Li, and R. Yang, "Four-dimensional SAR imaging scheme based on compressive sensing," *Progress In Electromagnetics Research B*, Vol. 39, 225–239, 2012.
104. Haldar, D., C. Patnaik, S. Mohan, and M. Chakraborty, "Jute and tea discrimination through fusion of SAR and optical data," *Progress In Electromagnetics Research B*, Vol. 39, 337–354, 2012.
105. Feng, J., Z. Cao, and Y. Pi, "Variational SAR image segmentation based on the G^0 model and an augmented Lagrangian method," *Progress In Electromagnetics Research B*, Vol. 39, 373–392, 2012.
106. Ren, X.-Z., Y. Qin, and L. H. Qiao, "Interferometric properties

and processing for spaceborne spotlight SAR," *Progress In Electromagnetics Research B*, Vol. 36, 267–281, 2012.

107. Haldar, D., A. Das, S. Mohan, O. Pal, R. S. Hooda, and M. Chakraborty, "Assessment of L-band SAR data at different polarization combinations for crop and other landuse classification," *Progress In Electromagnetics Research B*, Vol. 36, 303–321, 2012.
108. Yanase, K. and A. Hirata, "Effective resistance of grounded humans for whole-body averaged SAR estimation at resonance frequencies," *Progress In Electromagnetics Research B*, Vol. 35, 15–27, 2011.
109. Gangwar, R. K., S. P. Singh, and D. Kumar, "SAR distribution in a bio-medium in close proximity with rectangular dielectric resonator antenna," *Progress In Electromagnetics Research B*, Vol. 31, 157–173, 2011.
110. Golezani, J. J., M. Abbak, and I. Akduman, "Modified directional wide band printed monopole antenna for use in radar and microwave imaging applications," *Progress In Electromagnetics Research Letters*, Vol. 33, 119–129, 2012.
111. Tan, W., W. Hong, Y. Wang, and Y. Wu, "A novel spherical-wave three-dimensional imaging algorithm for microwave cylindrical scanning geometries," *Progress In Electromagnetics Research*, Vol. 111, 43–70, 2011.
112. AlShehri, S. A., S. Khatun, A. B. Jantan, R. S. A. Raja Abdullah, R. Mahmood, and Z. Awang, "Experimental breast tumor detection using NN-based UWB imaging," *Progress In Electromagnetics Research*, Vol. 111, 447–465, 2011.
113. Bonafoni, S., F. Alimenti, G. Angelucci, and G. Tasselli, "Microwave radiometry imaging for forest fire detection: A simulation study," *Progress In Electromagnetics Research*, Vol. 112, 77–92, 2011.
114. Giamalaki, M. I. and I. S. Karanasiou, "Enhancement of a microwave radiometry imaging system's performance using left handed materials," *Progress In Electromagnetics Research*, Vol. 117, 253–265, 2011.
115. Wei, S.-J., X.-L. Zhang, and J. Shi, "Linear array SAR imaging via compressed sensing," *Progress In Electromagnetics Research*, Vol. 117, 299–319, 2011.
116. Liu, Q., W. Hong, W. Tan, Y. Lin, Y. Wang, and Y. Wu, "An improved polar format algorithm with performance analysis for geosynchronous circular SAR 2D imaging," *Progress In Electromagnetics Research*, Vol. 119, 155–170, 2011.

117. Ren, X.-Z., L. H. Qiao, and Y. Qin, "A three-dimensional imaging algorithm for tomography SAR based on improved interpolated array transform1," *Progress In Electromagnetics Research*, Vol. 120, 181–193, 2011.
118. An, D. X., Z.-M. Zhou, X.-T. Huang, and T. Jin, "A novel imaging approach for high resolution squinted spotlight SAR based on the deramping-based technique and azimuth NLCS principle," *Progress In Electromagnetics Research*, Vol. 123, 485–508, 2012.
119. Martnez-Lorenzo, J. A., F. Quivira, and C. M. Rappaport, "SAR imaging of suicide bombers wearing concealed explosive threats," *Progress In Electromagnetics Research*, Vol. 125, 255–272, 2012.
120. Chen, J., J. Gao, Y. Zhu, W. Yang, and P. Wang, "A novel image formation algorithm for high-resolution wide-swath spaceborne SAR using compressed sensing on azimuth displacement phase center antenna," *Progress In Electromagnetics Research*, Vol. 125, 527–543, 2012.
121. Liao, K.-F., X.-L. Zhang, and J. Shi, "Fast 3-D microwave imaging method based on subaperture approximation," *Progress In Electromagnetics Research*, Vol. 126, 333–353, 2012.
122. Yang, W., Y. Liu, G.-S. Xia, and X. Xu, "Statistical mid-level features for building-up area extraction from full polarimetric SAR imagery," *Progress In Electromagnetics Research*, Vol. 132, 233–254, 2012.
123. Zhang, Y., W. Zhai, X. Zhang, X. Shi, X. Gu, and Y. Deng, "Ground moving train imaging by KU-band radar with two receiving channels," *Progress In Electromagnetics Research*, Vol. 130, 493–512, 2012.
124. Chen, J., Z. Li, and C.-S. Li, "A novel strategy for topside ionosphere sounder based on spaceborne MIMO radar with FBCD," *Progress In Electromagnetics Research*, Vol. 116, 381–393, 2011.
125. Liu, J., X. Li, S. Xu, and Z. Zhuang, "ISAR imaging of non-uniform rotation targets with limited pulses via compressed sensing," *Progress In Electromagnetics Research B*, Vol. 41, 285–305, 2012.
126. He, X.-Y., X.-B. Wang, X. Zhou, B. Zhao, and T.-J. Cui, "Fast ISAR image simulation of targets at arbitrary aspect angles using a novel SBR method," *Progress In Electromagnetics Research B*, Vol. 28, 129–142, 2011.
127. Bullardm, B. D. and P. C. Dowdy, "Pulse Doppler signature of a rotary-wing aircraft," *IEEE Aerospace and Electronic Systems*

Magazine, Vol. 6, 28–30, 1991.

128. Yoon, S.-H., B.-W. Kim, and Y.-S. Kim, "Helicopter classification using time-frequency analysis," *Electronics Letters*, Vol. 36, 1871–1872, 2000.
129. Wu, D., Z. Xu, L. Zhang, Z. Xiong, and S. Xiao, "Performance analysis of polarization-space-time three-domain joint processing for clutter suppression in airborne radar," *Progress In Electromagnetics Research*, Vol. 129, 579–601, 2012.
130. Wu, J., J. Yang, Y. Huang, Z. Liu, and H. Yang, "A new look at the point target reference spectrum for bistatic SAR," *Progress In Electromagnetics Research*, Vol. 119, 363–379, 2011.
131. Chen, H.-W., J. Ding, X. Li, and Z. Zhuang, "MIMO radar systems design based on maximum channel capacity," *Progress In Electromagnetics Research B*, Vol. 34, 313–326, 2011.
132. Nguyen, N. T. M., D. Lautru, and H. Roussel, "A 3D model to characterize high-frequency scattering by urban areas for monostatic and bistatic radar configurations," *Progress In Electromagnetics Research B*, Vol. 30, 83–102, 2011.
133. Chen, H.-W., X. Li, J. Yang, W. Zhou, and Z. Zhuang, "Effects of geometry configurations on ambiguity properties for bistatic MIMO radar," *Progress In Electromagnetics Research B*, Vol. 30, 117–133, 2011.
134. Yang, M. and G. Zhang, "Compressive sensing based parameter estimation for monostatic MIMO noise radar," *Progress In Electromagnetics Research Letters*, Vol. 30, 133–143, 2012.
135. Escot-Bocanegra, D., D. Poyatos-Martnez, I. Montiel-Sanchez, F. M. Saez de Adana, and I. Gonzalez-Diego, "Spherical indoor facility applied to bistatic radar cross section measurements," *Progress In Electromagnetics Research Letters*, Vol. 26, 181–187, 2011.
136. Yu, X., L. Wang, H.-G. Wang, X. Wu, and Y.-H. Shang, "A novel multiport matching method for maximum capacity of an indoor MIMO system," *Progress In Electromagnetics Research*, Vol. 130, 67–84, 2012.
137. Bencheikh, M. L. and Y. Wang, "Combined ESPRIT-ROOTMUSIC for DOA-DOD estimation in polarimetric bistatic MIMO radar," *Progress In Electromagnetics Research Letters*, Vol. 22, 109–117, 2011.
138. Sirenko, K., V. Pazynin, Y. K. Sirenko, and H. Baci, "Compression and radiation of high-power short RF pulses. I. Energy accumulation in direct-flow waveguide compressors,"

Progress In Electromagnetics Research, Vol. 116, 239–270, 2011.

139. Galati, G. and G. Pavan, "Range sidelobes suppression in pulse-compression radar using Golay pairs: Some basic limitations for complex targets," *IEEE Transactions on Aerospace and Electronic Systems*, Vol. 48, 2756–2760, 2012.
140. Akbaripour, A. and M. H. Bastani, "Range sidelobe reduction filter design for binary coded pulse compression system," *IEEE Transactions on Aerospace and Electronic Systems*, Vol. 48, 348–359, 2012.
141. Lin, Li, A. E.-C. Tan, K. Jhamb, and K. Rambabu, "Buried object characterization using ultra-wideband ground penetrating radar," *IEEE Transactions on Microwave Theory and Techniques*, Vol. 60, 2654–2664, 2012.
142. Wong, S.-K., F. Kung Wai Lee, S. Maisurah, and M. N. B. Osman, "A WiMedia compliant CMOS RF power amplifier for ultra-wideband (UWB) transmitter," *Progress In Electromagnetics Research*, Vol. 112, 329–347, 2011.
143. Zhang, Z. and Y. H. Lee, "A robust cad tool for integrated design of UWB antenna system," *Progress In Electromagnetics Research*, Vol. 112, 441–457, 2011.
144. Saleem, R. and A. K. Brown, "Empirical miniaturization analysis of inverse parabolic step sequence based UWB antennas," *Progress In Electromagnetics Research*, Vol. 114, 369–381, 2011.
145. Lizzi, L., G. Oliveri, and A. Massa, "A time-domain approach to the synthesis of UWB antenna systems," *Progress In Electromagnetics Research*, Vol. 122, 557–575, 2012.
146. McGinley, B., M. O'Halloran, R. C. Conceicao, G. Higgins, E. Jones, and M. Glavin, "The effects of compression on ultra wideband radar signals," *Progress In Electromagnetics Research*, Vol. 117, 51–65, 2011.
147. Zhu, C.-H., Q. H. Liu, Y. Liu, Y. Shen, and L. J. Liu, "An accurate conformal Fourier transform method for 2D discontinuous functions," *Progress In Electromagnetics Research*, Vol. 120, 165–179, 2011.
148. Vicen-Bueno, R., M. Rosa-Zurera, M. P. Jarabo-Amores, and D. De La Mata-Moya, "Coherent detection of Swerling 0 targets in sea-ice Weibull-distributed clutter using neural networks," *IEEE Transactions on Instrumentation and Measurement*, Vol. 59, No. 12, 3139–3151, 2010.
149. Vicen-Bueno, R., R. Carrasco-Alvarez, M. Rosa-Zurera, J. C. Nieto-Borge, and M. P. Jarabo-Amores, "Artificial neural

network-based clutter reduction systems for ship size estimation in maritime radars," *EURASIP Journal on Advances in Signal Processing*, Vol. 2010, 380473, 1–15, 2010.

150. Habib, M. A., M. Barkat, B. Aissa, and T. A. Denidni, "CA-CFAR detection performance of radar targets embedded in non-centered chi-2 gamma clutter," *Progress In Electromagnetics Research*, Vol. 88, 135–148, 2008.
151. Gao, G., L. Liu, L. Zhao, C. Shi, and G. Kuang, "An adaptive and fast CFAR algorithm based on automatic censoring for target detection in high-resolution SAR images," *IEEE Transactions on Geoscience and Remote Sensing*, Vol. 47, No. 6, 1685–1697, 2009.
152. Vicen-Bueno, R., R. Carrasco-Alvarez, M. P. Jarabo-Amores, J. C. Nieto-Borge, and E. Alexandre-Cortizo, "Detection of ships in marine environments by square integration mode and multilayer perceptrons," *IEEE Transactions on Instrumentation and Measurement*, Vol. 60, No. 3, 712–724, 2011.
153. Vicen-Bueno, R., R. Carrasco-Alvarez, M. P. Jarabo-Amores, J. C. Nieto-Borge, and M. Rosa-Zurera, "Ship detection by different data selection templates and multilayer perceptrons from incoherent maritime radar data," *IET Radar, Sonar and Navigation*, Vol. 5, No. 2, 144–154, 2011.
154. Mohammadpoor, M., R. S. A. Raja Abdullah, A. Ismail, and A. F. Abas, "A circular synthetic aperture radar for on-the-ground object detection," *Progress In Electromagnetics Research*, Vol. 122, 269–292, 2012.
155. Vicen-Bueno, R., M. Rosa-Zurera, M. P. Jarabo-Amores, and R. Gil-Pita, "Automatic target detection in simulated ground clutter (Weibull distributed) by multilayer perceptrons in a low-resolution coherent radar," *IET Radar, Sonar and Navigation*, Vol. 4, No. 2, 315–328, 2010.
156. Baum, C., "On the singularity expansion method for the solution of electromagnetic interaction problems," Air Force Weapons Lab, 1971.
157. Baum, C., "Singularity expansion of electromagnetic fields and potentials radiated from antennas or scattered from objects in free space," Air Force Weapons Lab, 1973.
158. Baum, C., "The singularity expansion method," *Transient Electromagnetic Fields*, Vol. 10, 129–179, 1976.
159. Baum, C., E. Rothwell, K. Chen, and D. Nyquist, "The singularity expansion method and its application to target identification," *Proceedings of the IEEE*, Vol. 79, 1481–1492, Oct. 1991.

160. Lee, J.-H. and H. T. Kim, "Radar target recognition based on late time representation: Closed-form expression for criterion," *IEEE Transactions Antennas and Propagation*, Vol. 54, 2455–2462, Sep. 2006.
161. Lee, J.-H. and H.-T. Kim, "Radar target recognition using least squares estimate," *Microwave and Optical Technology Letters*, Vol. 30, 427–434, Sep. 2001.
162. Mooney, J. E., Z. Ding, and L. S. Riggs, "Performance analysis of a GLRT automated target discrimination scheme," *IEEE Transactions Antennas and Propagation*, Vol. 49, No. 12, 1827–1835, Dec. 2001.
163. Morales, J. D., D. Blanco, D. P. Ruiz, and M. C. Carrion, "Non cooperative radar target identification using exponential single-mode extraction pulse," *IEEE Transactions on Antennas and Propagation*, Vol. 59, No. 6, 2445–2447, 2011.
164. Lee, W. J., T. K. Sarkar, H. S. Moon, and L. Brown, "Detection and identification using natural frequency of the perfect electrically conducting (PEC) sphere in the frequency and time domain," *IEEE International Symposium on Antennas and Propagation*, 2334–2337, 2011.
165. Chauveau, J., D. Beaucoudrey, and N. J. Saillard, "Resonance behavior of radar targets with aperture: Example of an open rectangular cavity," *IEEE Transactions on Antennas and Propagation*, Vol. 58, 2060–2068, 2010.
166. Aldhubaib, F., H.-S. Lui, and N. V. Shuley, "A radar target signature based on resonance and dual polarization features," *Microwave Conference*, 1–4, 2008.
167. Tesche, F., "On the analysis of scattering and antenna problem using the singularity expansion method," *IEEE Transactions Antennas and Propagation*, Vol. 21, 53–62, Jan. 1973.
168. Lee, J.-H., S.-W. Cho, S.-H. Park, and K.-T. Kim, "Performance analysis of radar target recognition using natural frequency: Frequency domain approach," *Progress In Electromagnetics Research*, Vol. 132, 315–345, 2012.
169. Lee, J.-H. and S.-H. Jeong, "Performance of natural frequency-based target detection in frequency domain," *Journal of Electromagnetic Waves and Applications*, Vol. 26, Nos. 17–18, 2426–2437, 2012.
170. Horn, R. A. and C. R. Johnson, *Matrix Analysis*, Cambridge Univ. Press, Cambridge, UK, 1986.